

Article

Calibration of Ramie Stalk Contact Parameters Based on the Discrete Element Method

Yao Hu [†], Wei Xiang [†], Yiping Duan, Bo Yan, Lan Ma , Jiajie Liu and Jiangnan Lyu ^{*}

Institute of Bast Fiber Crops, Chinese Academy of Agricultural Sciences, Changsha 410205, China; 82101202102@caas.cn (Y.H.); xiangwei@caas.cn (W.X.); hunaudyp@stu.hunau.edu.cn (Y.D.); yanbo@caas.cn (B.Y.); malan@caas.cn (L.M.); liujiajie@caas.cn (J.L.)

^{*} Correspondence: yjljn@sina.com

[†] These authors contributed equally to this work.

Abstract: To obtain the physical parameters and contact parameters of ramie stalk decorticating simulation, the structural dimensions, density, moisture content, elastic modulus, and contact parameters of the ramie stalk were measured in this study based on the phloem and xylem of the ramie stalk. The physical stacking angles of the phloem and xylem were measured by the cylinder lift method and the extraction of the partition method, respectively. The contact parameters between the xylem and phloem of the ramie stalk were directly calibrated. Additionally, the contact parameters of the phloem–phloem, phloem–Q235A steel, xylem–xylem, and xylem–Q235A steel were used as calibration objects, and the simulated stacking angle was used as the evaluation index. Then, the Plackett–Burman test was designed to screen for the parameters which were significantly affecting the simulated stacking angle. Furthermore, the steepest ascent test determined the optimal range of values for two significant parameters of the phloem and three significant parameters of the xylem. Based on the central composite design, the second-order regression equations between the significant parameters of the phloem and xylem and the stacking angle were established, respectively. The physical stacking angles of 37.93° for phloem and 27.17° for xylem were the target values to obtain the optimal parameter group. The results showed that the restitution, static, and rolling friction coefficients between the xylem and phloem were 0.60, 0.53, and 0.021, respectively. The static and rolling friction coefficients between the phloem and phloem were 0.41 and 0.056, respectively. The rolling friction coefficient between the xylem and Q235A steel was 0.033, and the static and rolling friction coefficients between the xylem and xylem were 0.44 and 0.016, respectively. The verification test showed that the relative error values were less than 2.11%, which further indicated that the modeling method and parameter calibration of the ramie stalk phloem and xylem models were accurate and reliable. They can be used for the subsequent calibration simulation tests of ramie stalk bonding parameters and ramie stalk decorticating simulations.

Keywords: ramie stalk; discrete element method (DEM); parameter calibration; stacking angle; contact parameters



Citation: Hu, Y.; Xiang, W.; Duan, Y.; Yan, B.; Ma, L.; Liu, J.; Lyu, J. Calibration of Ramie Stalk Contact Parameters Based on the Discrete Element Method. *Agriculture* **2023**, *13*, 1070. <https://doi.org/10.3390/agriculture13051070>

Academic Editor: Filipe Neves Dos Santos

Received: 7 April 2023

Revised: 18 April 2023

Accepted: 27 April 2023

Published: 17 May 2023



Copyright: © 2023 by the authors. Licensee MDPI, Basel, Switzerland. This article is an open access article distributed under the terms and conditions of the Creative Commons Attribution (CC BY) license (<https://creativecommons.org/licenses/by/4.0/>).

1. Introduction

Ramie is a culturally significant and traditional economic crop in China. It is widely cultivated in the Yangtze River Basin and southern China, with the planting area and fiber production accounting for over 95% of the global output [1]. Ramie is a perennial herbaceous plant belonging to the family Urticaceae [2], with its entire body being highly valuable. Its fiber exhibits excellent properties, such as strong moisture absorption, great breathability, antibacterial properties, and biodegradability [3–5], which makes it widely useful in textiles, medicine, military, agriculture, and ecofriendly packaging industries. However, the fiber of ramie must be decorticated and processed before use in the textile industry [6]. The ramie decorticator is the main processing equipment for decorticating

ramie fiber. The high-speed rotating rollers can crush and eject the xylem through bending and beating the ramie stalk frequently while at the same time keeping the bast fiber intact, thereby obtaining pure raw ramie fiber [7]. However, the movement of each component of the ramie stalk is complex during decorticating, and traditional research methods are unable to simulate and analyze this movement state, which has so far hindered the optimization of decorticating equipment.

Simulation technology is widely used to optimize agricultural machines due to the rapid development of computational speed [8,9]. The EDEM simulation software based on the discrete element method can accurately analyze the movement law of agricultural materials in agricultural machinery. In agricultural machinery simulation operations, agricultural materials can be modeled as particles or clusters. The EDEM software can record the real-time movement trajectory and mechanical behavior of agricultural materials and conduct in-depth research on the interaction mechanism between materials and machinery; this can guide the optimization of the machinery design [10,11]. However, it is crucial to input the accurate physical and contact parameters of the materials to establish a discrete element model, which can faithfully reproduce the characteristic properties of the material and adapt to the real-world operating conditions of the machinery.

The DEM simulation modeling requires the input of intrinsic physical and contact parameters [12]. Due to the individual differences in materials, errors in physical tests, and differences in model constructions, obtaining accurate discrete element parameters through physical tests is difficult. Therefore, the calibration of physical tests and virtual simulations must be conducted to ensure consistency between the simulation and physical results. A stacking angle test can effectively calibrate discrete element parameters [13]. Various stacking angle measurement methods have been developed for different material characteristics, such as the injection, tilted box, cylinder lifting, and extraction of partition methods [14–17]. These methods are widely used to calibrate discrete element simulation parameters in materials such as soil, fertilizer, seeds, and biomass stalks. Xiang et al. [18] built a soil simulation model based on soil stacking tests of physical measurements and EDEM-software-recommended parameters. They used the stacking angle as the response value and completed the calibration and optimization of soil simulation's physical parameters through the Plackett–Burman, steepest ascent, and Box–Behnken tests. Liu et al. [19] obtained the stacking angle of a wheat grain heap through physical and simulation tests under the response value of different parameter combinations, which were finally based on response surface optimization, and they calibrated the discrete element simulation parameters of wheat. Xiao et al. [20] explored the influence of compound fertilizer characteristic parameters on the stacking angle, and they determined the rolling friction coefficients of the three types of granular fertilizers under two particle modeling methods. Shi et al. [21] measured the interval values of the contact parameters of fallen jujube through stacking angle tests. They used EDEM software to establish a simulation test of a fallen jujube stacking angle. They used Plackett–Burman, steepest ascent, and central composite design tests to obtain specific values of simulation parameters from the interval values. Dai et al. [22] used 3D scanning technology to construct a discrete element model of lily bulbs, and they calibrated the contact parameters between the lily bulbs and Q235 steel through bench tests and simulation parameter tests, and then established a regression model for the relative errors of the parameters and optimized the response surface to calibrate the discrete element contact parameters of the lily bulbs. Zhang et al. [17] determined the contact parameters between corn stalks and shredder blades, as well as corn stalks themselves. They used the extraction of the partition method to calibrate the contact parameters for corn stalk discrete element simulation. The research on discrete element simulation modeling and the parameter calibration of agricultural materials mainly focuses on spherical and quasi-spherical particles, such as soil, crop seeds, and fertilizers, and large spherical particles, such as fruits and plant bulbs. Unlike traditional spherical and quasi-spherical particle materials, the ramie stalk has a cylindrical shape in its xylem, and its phloem is strip-shaped after

being decorticated from the xylem. Few scholars have studied the calibration of the contact parameters of discrete element models on the ramie stalk.

To establish a discrete element simulation model of ramie stalks, this study established the discrete element models of the phloem and xylem on ramie stalk through the physical and simulation tests. Based on the measurement results of the phloem and xylem of ramie stalks, the stacking angle of the phloem and xylem particle mixture was taken as the response value. This study employed Plackett–Burman, steepest ascent, and response surface tests to complete the calibration and optimization of the contact parameters of the phloem and xylem on ramie stalks. This can provide a basic model and technical support for simulating the decortivating process of ramie fiber.

2. Materials and Methods

2.1. Measurement of the Physical Parameters of Ramie Stalk Phloem and Xylem

We selected the “Zhongzhu No. 1” variety of ramie as the experimental object to measure the structural dimensions, density, shear modulus, and other parameters of the ramie stalk’s phloem and xylem. The “Zhongzhu No. 1” variety of ramie was planted at the Shijihu test base of Bast Fiber Crops of the Chinese Academy of Agricultural Sciences Institute in Yuanjiang City, Hunan Province.

2.1.1. Dimensional Measurements

We employed a five-point sampling method to obtain 100 random samples of ramie stalks. The plant height was measured using a tape measure (with an accuracy of 1 mm), and the xylem outer diameter, xylem inner diameter, and phloem thickness of the ramie stalk were measured using a DL91150 Vernier caliper (with an accuracy of 0.01 mm). The results are the average values of the measurements.

The results of the measurements are shown in Table 1. The average values of the ramie plant height, xylem outer diameter, xylem inner diameter, and phloem thickness were 1969.38 mm, 12.56 mm, 7.98 mm, and 0.71 mm, respectively.

Table 1. Structural dimensions of the ramie.

Parameters	Max/mm	Min/mm	Mean/mm	Standard Deviation/mm	Variance/mm
Plant height	2307.00	1457.00	1969.38	217.27	4.77×10^4
Xylem outer diameter	16.11	9.00	12.56	1.58	2.51
Xylem inner diameter	13.07	5.31	7.98	1.26	1.60
Phloem thickness	1.21	0.45	0.71	0.15	0.02

2.1.2. Density and Moisture Content

The density of the phloem and xylem of a fresh ramie stalk was measured using a liquid immersion method [23] by immersing a certain mass of phloem and xylem in water and measuring the drainage volume to obtain the volume of each component of the ramie stalk and then calculating its density. The test was repeated ten times, and the average value was taken. The average densities of the phloem and xylem were 1618.95 kg/m^3 and 751.50 kg/m^3 , respectively.

The moisture content of the ramie stalk was determined according to the “Method for determination of the moisture content of wood” [24] using a high-precision balance (with a weighing range of 220 g and an accuracy of 0.001 g) and a DGT-G220 blast drying oven. The moisture content of the ramie stalk was calculated to be approximately 79.72%.

2.1.3. Elastic Modulus and Shear Modulus

Tensile testing is a common method for obtaining the elastic modulus. This method has been used to measure the elastic modulus of wood [25], corn straw [26], rice stalk [27],

bamboo stalk [28], and reed stalk [29], providing the most concentrated measurement of the elastic modulus [30]. In this study, based on the standard “Method of sample logs sawing and test specimens selection for physical and mechanical tests of wood” [31] and the relevant literature [32], tensile tests of the phloem and xylem of the ramie stalks were performed using a microcomputer-controlled electronic universal material testing machine (produced by Shanghai Tuofeng Instruments Co., Ltd., Shanghai, China), model TFW-508, with a 500 N transducer, and the accuracies of the force transducer as well as the displacement transducer were within $\pm 0.1\%$. The test parameters were set to a loading speed of 5 mm/min. The stopping condition was judged to be a drop in the force value of more than 80% of the peak force. The tensile test is shown in Figure 1. The elastic modulus was calculated based on the slope of the linear region of the stress–strain curve. The shear modulus was derived from the elastic modulus using a conversion formula.

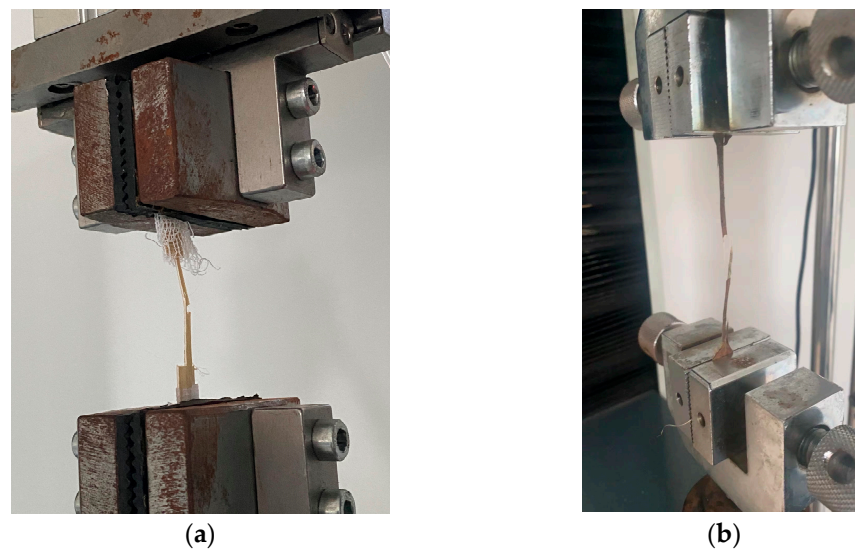


Figure 1. Tensile test to determine the modulus of elasticity: (a) xylem tensile test; (b) phloem tensile test.

The results show that the average elastic modulus of the phloem and xylem were 1721.4 MPa and 630.3 MPa, respectively. The average shear modulus values of the phloem and xylem were calculated to be 614.8 MPa and 242.4 MPa, respectively, using Equation (1):

$$\begin{cases} E = \frac{F_1}{\delta A} \\ \varepsilon = \lim_{T_1 \rightarrow 0} \frac{\Delta L}{L_1} \\ G = \frac{E}{2(1+\nu)} \end{cases} \quad (1)$$

where E represents the elastic modulus of ramie, MPa; F_1 represents the axial load on ramie, N; A represents the contact area, mm^2 ; ε represents the strain value; ΔL represents the deformation of the ramie after tension, mm; L represents the length of the tensile area of the ramie specimen, mm; G represents the shear modulus, MPa; and ν is the Poisson’s ratio.

2.2. Method for Determining Contact Parameters

The contact parameters of the ramie stalk discrete element simulation model included the coefficient of restitution, coefficient of static friction, coefficient of rolling friction between the phloem and phloem, phloem and Q235A steel, phloem and xylem, xylem and xylem, and xylem and Q235A steel. Among them, the physical tests mainly measured the contact parameters between the phloem and Q235A steel, phloem and xylem, and xylem and Q235A steel. As the phloem–phloem and xylem–xylem contact parameters are difficult to obtain directly from physical tests, physical tests of the stacking angle of phloem

and xylem needed to be carried out and calibrated by subsequent simulation tests of the stacking angle.

2.2.1. Coefficient of Restitution

In this study, we mainly measured the coefficient of restitution between phloem and Q235A steel, xylem and Q235A steel, and phloem and xylem. The coefficient of restitution is a parameter that measures the ability of an object to return to its original shape after a collision. It is defined as the ratio of the normal relative separation velocity after a collision to the relative approach velocity before collision (i.e., the ratio of the highest rebound height (h') and the initial drop height (h) during the collision between the test object and the material) [33]. When an object falls freely and collides with the test object, the object bounces freely after the collision, and only gravity works during the falling and rising process. The formula for calculating the coefficient of restitution is as follows (2):

$$e = \left| \frac{v'_2 - v'_1}{v_1 - v_2} \right| = \left| \frac{-\sqrt{2gh'}}{\sqrt{2gh}} \right| = \sqrt{\frac{h'}{h}} \quad (2)$$

where v_1 and v_2 are the velocities of the test object and the material before collision, m/s; v'_1 and v'_2 are the velocities of the test object and the material after collision, m/s; h and h' are the initial drop height and the highest rebound height, mm; and g is the acceleration due to the fact of gravity, m/s².

The maximum rebound height of the coefficient of restitution can be measured using a high-speed camera system. The experimental process was recorded by connecting the high-speed camera, HiSpec5 (Fastec Imaging Inc., San Diego, CA, USA) to a computer. The camera was set to a frequency of 500 Hz, with a resolution of 1280 × 1024 pixels, and a sampling rate of 2 ms. Considering that the ramie stalk has a lower density, the air resistance significantly impacts the experimental results when the falling speed is high. Therefore, the object to be measured was dropped freely from an initial height (h) of 205 mm, collided with the contact material, and the highest rebound height (h') was captured and recorded. The experimental process is shown in Figure 2.

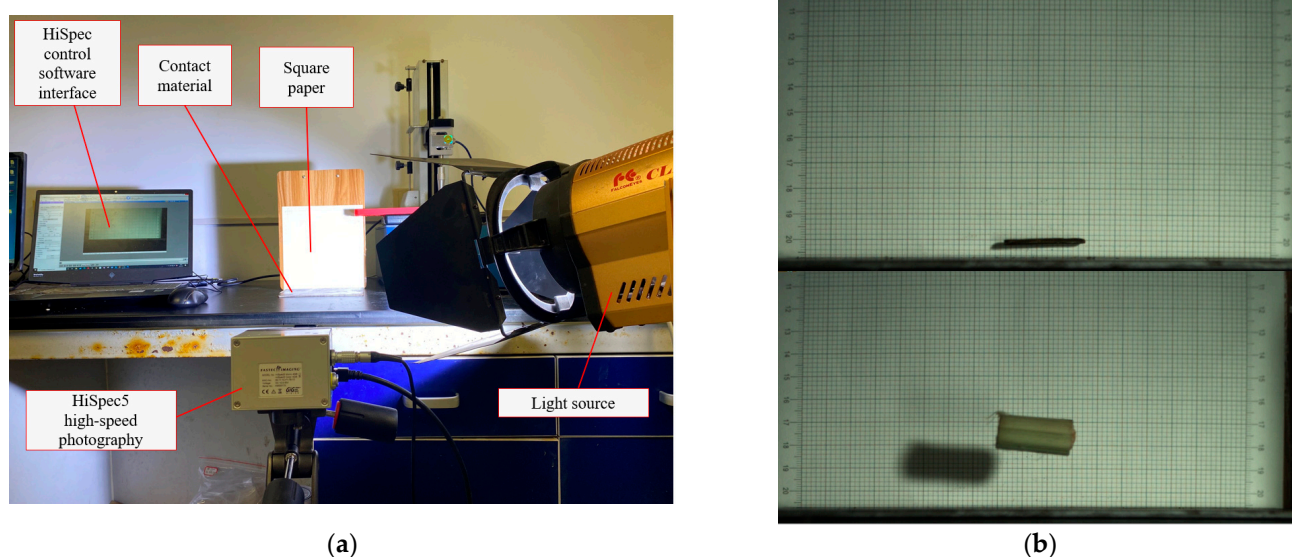


Figure 2. Measurement of the restitution coefficient: (a) test equipment; (b) keyframe of the rebound's highest point.

The rebound height (h') was recorded by capturing the keyframe when the tested object reached the highest position after the collision, from which the coefficient of restitution was calculated. Each group of tests was repeated ten times to analyze the positive collision

process between the phloem and Q235A steel, xylem and Q235A steel, and phloem and xylem, the coefficient of restitution was then calculated according to Equation (2), and the average value was taken.

2.2.2. Coefficient of Friction

Measurement of the Static Friction Coefficient

In this study, we mainly measured the static friction coefficients of phloem–Q235A steel, xylem–Q235A steel, and phloem–xylem. The static friction coefficient is the ratio of the maximum static friction force applied to the object to the normal pressure. It is usually measured by the incline plane method [34,35]. The ramie stalk with a high degree of roundness was selected, and the phloem was peeled with a cutter knife to create the test sample. A self-made inclinometer and a digital angle measuring instrument (accuracy of 0.05°) were used to measure and calculate the required static friction coefficient, as shown in Figure 3.

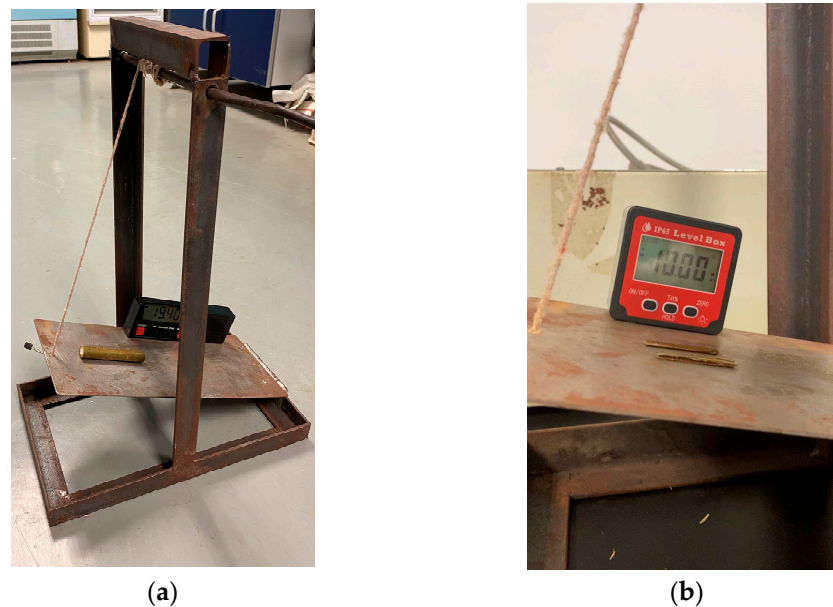


Figure 3. Measurement of the static friction coefficient: (a) test equipment; (b) sliding angle.

The test object was placed on a steel plate when the static friction coefficients of the ramie stalks for phloem–Q235A steel and the xylem–Q235A steel were measured. The handle of the inclinometer was shaken to raise the incline angle, and the sliding angle was recorded when a sliding trend occurred. When measuring the static friction coefficient of the phloem–xylem, the phloem was attached to the steel plate, and the xylem was axially placed above it for the test. The sliding angle was recorded, and the coefficient of static friction was calculated. The calculation of the static friction coefficient is shown in Equation (3):

$$\mu_1 = \frac{f}{F_2} = \frac{mgsina}{mgcosa} = \tan \alpha \quad (3)$$

where μ_1 is the static friction coefficient, f is the static friction force between the object and the inclined plane, N; F_2 is the force perpendicular to the inclined plane, N; m is the measured material mass, g; and α is the inclination angle, $^\circ$.

Measurement of the Rolling Friction Coefficient

The coefficient of rolling friction pertains to the deformation-induced resistance when an object rolls or tends to roll without slipping on another surface [36]. The experimental setup and method for measuring the rolling friction coefficients in this study were the same as those for measuring the static friction coefficients. According to the rolling friction

coefficient measurement method provided in the literature [37,38], the test object was placed radially on the test plate. The handle of the inclinometer was shaken to raise the inclination angle of the test plate, and the rolling angle was recorded when the test object showed a rolling trend. The coefficient of rolling friction coefficient was then calculated. When measuring the rolling friction coefficient between phloem–Q235A steel, a high-roundness ramie stalk was selected, and rolling was achieved by external phloem contact. When measuring the rolling trend between the phloem and xylem, the phloem was peeled off in advance and glued to the steel plate. The xylem was placed radially on the phloem plate, the inclination angle was increased, and the rolling friction coefficient was calculated.

2.3. Physical Test of the Stacking Angle

The stacking angle is a microparameter that characterizes the granular materials' flow and friction characteristics. Its numerical value is related to the material type, surface shape, and moisture content, and it is affected by the coefficient of restitution and the coefficient of friction [39]. The stacking angle test is usually used to calibrate discrete element parameters of granular materials. Therefore, we conducted a physical test of the stacking angle. The measurement results can calibrate the contact parameters between phloem and Q235A steel, phloem and phloem, xylem and Q235A steel, and xylem and xylem.

Through preliminary comparative tests, the cylindrical lifting method was found to be suitable for measuring the phloem's stacking angle, and the extraction of the partition method was suitable for measuring the stacking angle for the xylem.

Due to the ramie phloem fibers' lengthy and highly flexible nature, forming a stacking angle is difficult. We referred to the material processing method for calibrating the discrete element parameters of sugarcane leaves [40] and tobacco rods [16], and the phloem was peeled from the ramie stalks with a utility knife and trimmed into 5.6×5.6 mm specimens without altering the surface shape of the material. The stacking angle method for the ramie phloem was the cylinder lifting method, where a 20 g sample was placed into a steel cylinder with a diameter of 45 mm and a height of 57 mm. The cylinder was then lifted at a uniform speed of 4 mm/s using a TFW-508 mechanical universal testing machine, and the phloem sample fell onto a $250 \text{ mm} \times 250 \text{ mm} \times 2 \text{ mm}$ (length \times width \times thickness) steel plate from the bottom of the cylinder. After all phloem specimens had come to a complete stop, a stable phloem material pile was formed. The Canon EOS 70D DSLR camera was used to capture the main view of the phloem material pile from 50 cm in front of the pile, as shown in Figure 4a.



Figure 4. Physical test of the stacking angle: (a) stacking angle of the phloem; (b) stacking angle of the xylem.

For the xylem, a ramie stalk xylem radial stacking angle measurement device with removable partitions was created based on reference [17]. The device was made of Q235A steel and had dimensions of $500 \text{ mm} \times 200 \text{ mm} \times 300 \text{ mm}$ for the length, width, and height, respectively. To measure the xylem, the ramie stalk sheath was removed, and the phloem was peeled entirely clean. All xylem lengths were controlled at approximately 140 mm. A certain number of xylem stalks were placed into one side of the radial stacking angle

measurement device. The entire ramie xylem stalk was moved to the other side after the partition was vertically lifted, forming a radial stacking angle upon collision with the wall. The main view of the radial stacking angle formed after the movement of the xylem stalks was captured using the Canon EOS 70D DSLR camera, as shown in Figure 4b.

2.4. Discrete Element Virtual Simulation Test

2.4.1. Selection of the Contact Model

In this study, Q235A steel was used as the contact material for both the ramie phloem and ramie xylem in the physical tests. Since there was no adhesion between the phloem and xylem and the steel plate during the physical tests, and there was no significant deformation during the accumulation process, the phloem and xylem were idealized as rigid bodies without considering their mechanical properties, only exploring their contact relationship. Therefore, the Hertz–Mindlin (no slip) contact model was selected for the discrete element simulation. The contact parameters included the coefficient of restitution, coefficient of static friction, and coefficient of rolling friction between the phloem and Q235A steel, phloem and phloem, phloem and xylem, xylem and Q235A steel, and xylem and Q235A xylem.

2.4.2. Establishment of the Discrete Element Model for Ramie Stalk

Analysis of the Ramie Stalk Model

An analysis of the ramie stalk structure's composition was conducted to establish a discrete element model for the ramie stalk. The cross-section of the ramie stalk was approximately circular, with the outer to inner cross-sections consisting of the green husk layer, phloem, xylem, and central medulla, as shown in Figure 5. The central medulla is foam-like, with a loose tissue structure and irregular shape. At the same time, the green husk layer was very thin and brittle, both of which have negligible mechanical properties compared to other components.

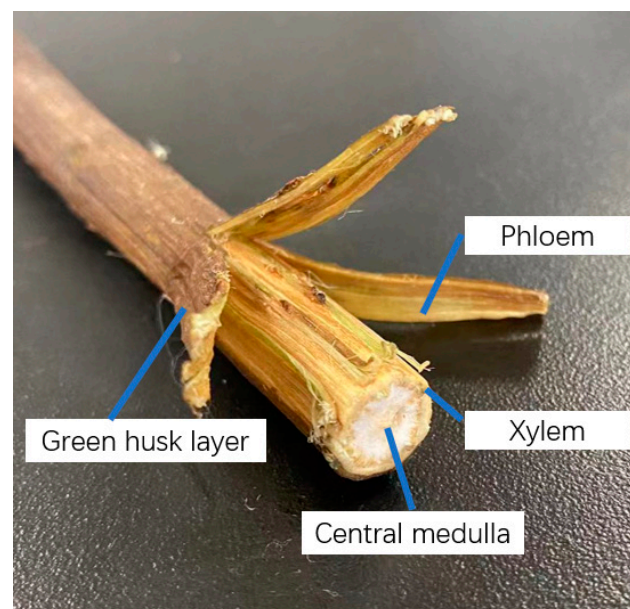


Figure 5. Schematic diagram of the structural composition of the ramie stalks.

Mechanical decortication of ramie stalks is performed by rolling and crushing the xylem with a roller to separate the xylem from the phloem, indicating that the breaking strength of the xylem was less than that of the phloem. From this apparent perspective, it can be assumed that the material properties of the green husk layer and the central medulla can be ignored, and the ramie stalk can be regarded as a combination of phloem and xylem materials. Therefore, only the phloem and xylem should be considered when a discrete

element model for the ramie stalk is established. The geometric model is shown in Figure 6. In this paper, the phloem was a composite of the green husk layer and the phloem fibers, and the physical tests did not remove the green husk layer.

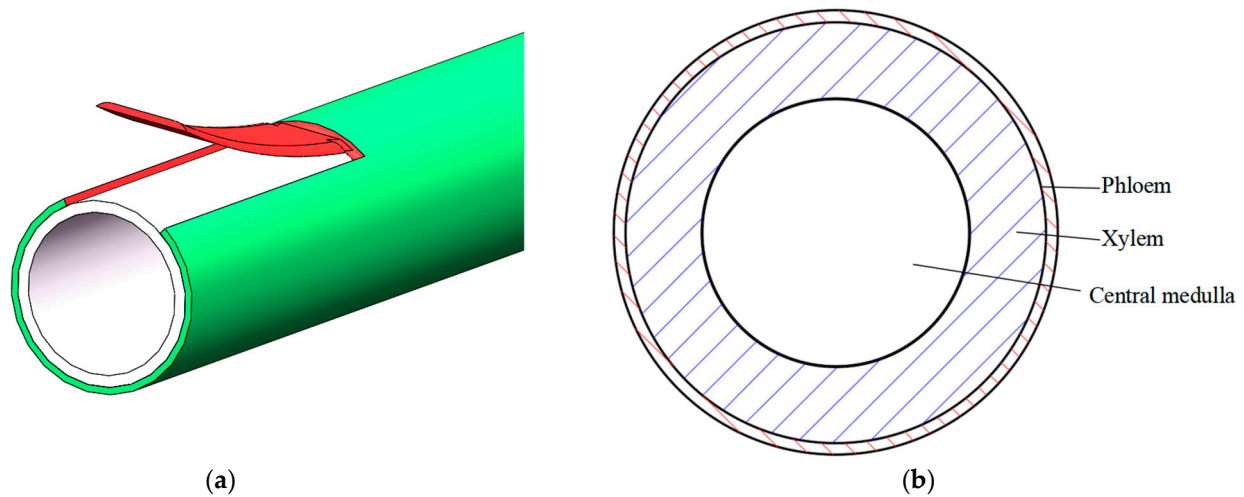


Figure 6. Ramie stalk geometry model: (a) ramie stalk structure simulation; (b) idealized cross-section of the ramie stalk.

Establishment of a Discrete Element Model for Ramie Stalk Phloem and Xylem

Simulation tests require the first step of building an accurate particle model. Ramie stalk phloem and xylem are nonspherical, and in DEM simulations, the multispherical method is usually used to construct irregular particle models [41–44]. In nonspherical particle discrete element simulations, the multichemical packing model has the advantages of fast calculation rate and simple contact judgment; however, as the number of filling particle elements increases, the simulation time will greatly increase, so the number of filling particle elements needs to be reasonable [45,46].

Since no significant deformation occurs during stacking, this study did not consider introducing bonding. When building the model, the ramie stalk phloem and xylem are first modeled and meshed using the Mesh submodule in the Workbench module of ANSYS 16.0 software. Then, the saved .msh file is imported into Fluent. The coordinate file containing the mesh coordinate information is obtained by reading and compiling the source file CalcRadius.c through the userdefine module, followed by executing CalcRadiusVolume. The coordinate data of the model are then imported into the .xml file saved by EDEM software, and the particle coordinate import is completed by entering EDEM. Based on the size measurement results of the ramie xylem, 732 circular spheres with a radius of 1.15 mm are used to form a cylindrical ramie stalk xylem with an outer diameter and inner diameter of 12.8 mm and 8 mm, respectively, and a length of 140 mm, as shown in Figure 7a.

The related study [40] showed that when calibrating the parameters of the discrete element model if the modeling is performed exactly according to the actual size of the material, it will greatly prolong the simulation time, increase the computational volume, and thus reduce the simulation efficiency. The correct calibration of the discrete element model with a moderately enlarged particle radius can truly reflect the contact parameters of the target material. The ramie phloem was relatively thin, and the filling particles according to the actual size will result in a low simulation efficiency due to the large number of calculations. In the simulation, the thickness of the ramie phloem was doubled, and 16 circular spheres with a radius of 0.7 mm were used to form a rectangular ramie stalk phloem with a length and width of 5.6×5.6 mm and a height of 1.4 mm, as shown in Figure 7b. Since the thickness of the ramie phloem is magnified in the simulation, it needs to be redetermined. The mass of a single sphere particle remained unchanged, and the

radius was doubled, so the volume increased eight times, and the density was one-eighth of the physical test value of 1618.95 kg/m^3 , which is 202.37 kg/m^3 .

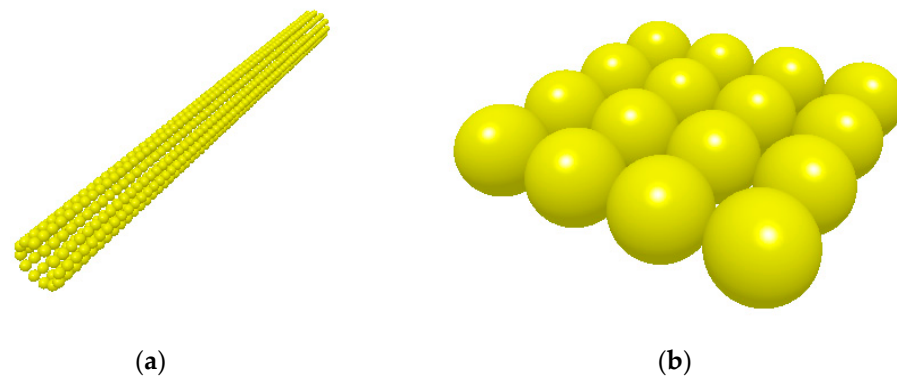


Figure 7. Ramie stalk discrete element model: (a) xylem discrete element model; (b) phloem discrete element model.

2.4.3. Calibration of Contact Parameters for Phloem–Xylem Discrete Element Model Calibration of the Phloem–Xylem Restitution Coefficient

In the physical measurement tests of phloem–xylem restitution coefficients, the coefficient was measured by the rebound height of the phloem and xylem attached to the steel plate. A discrete element simulation test was set up with the same experimental conditions. The collision simulation test was set with an initial collision height of 205 mm, a time step length of 20% of the Rayleigh time, and a save interval of 0.001 s. The rebound height was obtained by reading the data through the analyst module.

Calibration of the Phloem–Xylem Static Friction Coefficient

Based on the physical measurement results of the phloem–xylem static friction coefficient, discrete element simulation tests with the same experimental conditions were established. The friction test set the incline angle of the phloem plate to rise at a speed of 10 deg/s with a time step of 20% of the Rayleigh time and a save interval of 0.001 s. The sliding angle was obtained by reading the data through the discrete element analyst module.

Calibration of the Phloem–Xylem Rolling Friction Coefficient

Based on the physical measurement results of the phloem–xylem rolling friction coefficient, discrete element simulation tests with the same experimental conditions were established. The friction test set the incline angle of the phloem plate to rise at a speed of 10 deg/s with a time step of 20% of the Rayleigh time and a save interval of 0.001 s. The rolling angle was obtained by reading the data through the discrete element analyst module.

2.4.4. Calibration of the Discrete Element Parameters for the Stacking Angle Test

In the simulation of the stacking angle test for the phloem, the inner diameter and height of the cylinder were consistent with those used in the physical test. The interior of the cylinder was set as a particle factory, where the particles were generated freely by the “static” method. This ensured that the phloem was distributed in a relatively dispersed state inside the cylinder, avoiding a situation where an uneven distribution would result in a significant error in the stacking angle after being static. The total mass of the generated particles was 20 g. Subsequently, the particles were allowed to fall freely under gravity, and the simulation model was conducted for 1 s to reach a static equilibrium state. After, the cylinder was lifted vertically at a speed of 4 mm/s. The phloem particles would flow out slowly from the bottom of the cylinder, eventually forming a stable phloem particle heap on the bottom plate, as shown in Figure 8.

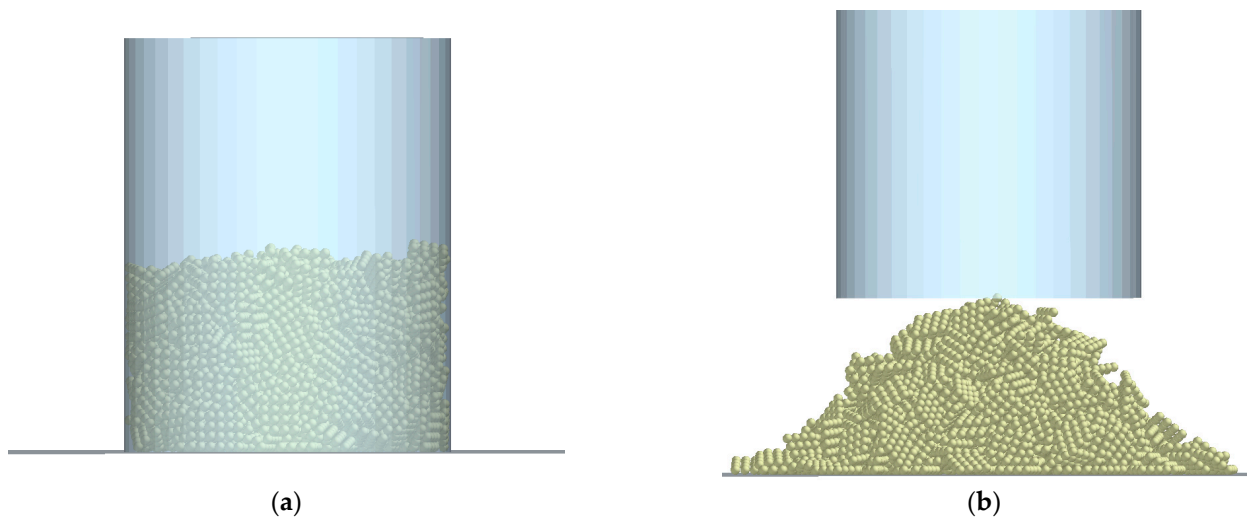


Figure 8. Ramie phloem stacking angle discrete element simulation test: (a) before stacking; (b) after stacking.

In the simulation of the stacking angle test for the xylem, the dimensions of the device and partition were consistent with those used in the physical test. Thirty-six neat piles of ramie xylem particles were generated at the right wall of the device. After the xylem particle heap and partition became stable, the partition was given a speed of 0.1 m/s to lift upward, and the xylem particle heap began to roll to the left to form the stacking angle. The discrete element simulation of the stacking angle test for the xylem is shown in Figure 9.

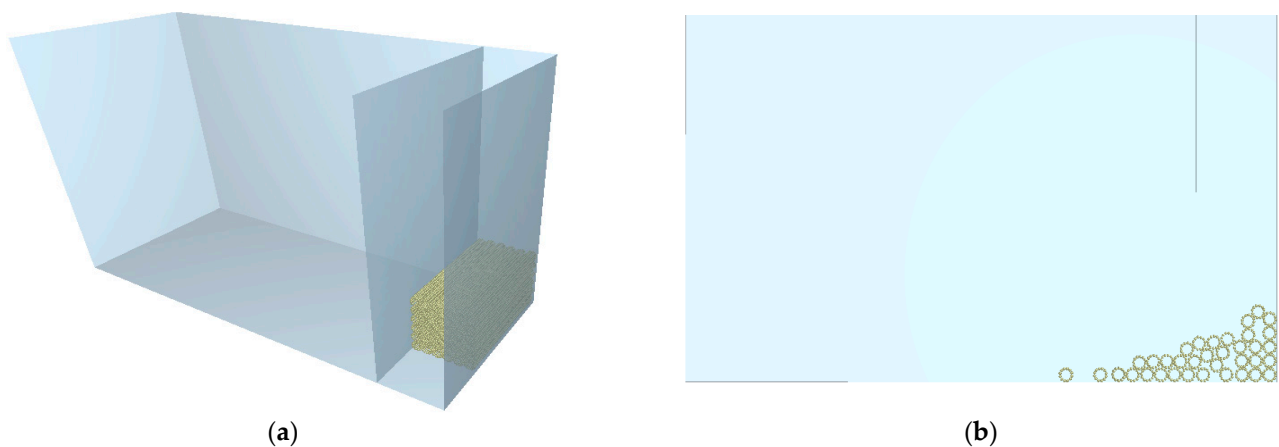


Figure 9. Ramie xylem stacking angle discrete element simulation test: (a) before stacking; (b) after stacking.

2.5. Discrete Element Simulation Test

In order to achieve a simulation model of the ramie stalk that matched its actual situation and ensured the reliability and authenticity of the model, this study used the Design-Expert 10.0.1 software to carry out tests, such as Plackett–Burman design, steepest ascent test design, and response surface design, to determine the key factors affecting the stacking angle in the simulation parameters of the ramie phloem and xylem, as well as the significant factor levels and parameter optimization of the ramie stalk phloem and xylem. Based on the fitting of the simulation stacking angle and the physical stacking angle of the ramie stalk phloem and xylem, the linear fitting method in MATLAB was used to compare the boundary pixel slope of the simulation model stacking angle and the actual material stacking angle to verify the accuracy of the model.

2.5.1. Plackett–Burman Design

To quickly screen the key factors affecting the response value of the stacking angle in the simulation parameters of ramie stalk phloem and xylem, this study used Design-Expert software to conduct a Plackett–Burman test analysis, taking the stacking angle of the phloem and xylem as the response value, using a 6-factor 2-level test method. The levels were represented in coded form, with a total of 13 groups of tests, each repeated twice, to compare the influence of each factor on the stacking angle of the phloem and xylem. The experimental plan is shown in Table 2.

Table 2. Plackett–Burman test program.

Phloem				Xylem			
Parameters	Symbols	Levels		Parameters	Symbols	Levels	
		Low level(−1)	High level(+1)			Low level(−1)	High level(+1)
Phloem–Q235A steel coefficient of restitution	X_1	0.05	0.45	Xylem–Q235A steel coefficient of restitution	X'_1	0.17	0.57
Phloem–Q235A steel coefficient of static friction	X_2	0.27	0.67	Xylem–Q235A steel coefficient of static friction	X'_2	0.36	0.76
Phloem–Q235A steel coefficient of rolling friction	X_3	0.005	0.100	Xylem–Q235A steel coefficient of rolling friction	X'_3	0.005	0.143
Phloem–Phloem coefficient of restitution	X_4	0.10	0.80	Xylem–Xylem coefficient of restitution	X'_4	0.10	0.80
Phloem–Phloem coefficient of static friction	X_5	0.10	0.60	Xylem–Xylem coefficient of static friction	X'_5	0.10	0.80
Phloem–Phloem coefficient of rolling friction	X_6	0.005	0.100	Xylem–Xylem coefficient of rolling friction	X'_6	0.005	0.050

A first-order polynomial linear model was used for the statistical modeling, as shown in Equation (4). The significance of each factor was obtained through variance analysis, and the significant influencing factors were selected.

$$\Omega = \sigma_0 + \sum_{k=1}^6 \sigma_k X_k \tag{4}$$

Here, Ω represents the stacking angle, °; σ_0 is the intercept of the model; σ_k is the linear coefficient; and X_k refers to the coded level of the independent variable.

2.5.2. Steepest Ascent Test Design

To screen the optimal parameter range of the significant factors in the phloem and xylem, Design-Expert software was used to conduct the steepest ascent test. During the simulation, based on the results of the Plackett–Burman test, the values of the nonsignificant factors were taken from the physical test values, and the values of the remaining factors were taken from the median values of the Plackett–Burman experimental levels. The significant factors were gradually increased according to the selected step size. The relative error between the measured results and the simulated stacking angle was analyzed until the minimum range of the upper and lower relative errors was selected as the basis for the response surface test value.

2.5.3. Response Surface Optimization Test and Regression Model Establishment

This study used the response surface analysis method to obtain the optimal parameter combination based on the results of the Plackett–Burman test and the steepest ascent test. The phloem and xylem were both using the central composite design method. Three significant levels (high, medium, and low) were taken from the results of the phloem and xylem climbing tests for the experimental design. The interaction effects of the significant factors on the stacking angle were analyzed.

2.5.4. Parameter Optimization and Validation

The Design-Expert software's Optimization module optimized the regression model with the experimental values of the stacking angle as the objective. The steepest ascent test determined the parameter optimization range, and a two-sample *t*-test was performed on the simulation and physical results. The reliability of the optimal combination of parameters was verified by checking whether there was a significant difference between the simulation and physical results.

3. Results and Discussion

3.1. Measurement Results of the Required Parameters for the DEM Simulation

Based on the physical parameter measurement results of the ramie stalk's phloem and xylem, combined with an analysis of the bounce-back process of the phloem and xylem using HiSpec Control Software, the experimental values of the restitution coefficient were obtained. The friction coefficient was calculated by recording the sliding and rolling angle, and the restitution coefficient and friction coefficient results are shown in Table 3.

Table 3. Parameters required for the discrete element simulation.

Parameter Type	DEM Parameter	Parameter Value	Source
Physical Parameters	Density of Q235A steel (kg/m ³)	7850	Literature [47]
	Shear modulus of Q235A steel (Pa)	7.90×10^{10}	Literature [47]
	Poisson's ratio of Q235A steel	0.30	Literature [47]
	Density of phloem (kg/m ³)	202.37	Section 2.1.2
	Shear modulus of phloem (Pa)	6.15×10^8	Section 2.1.3
	Poisson's ratio of phloem	0.40	Literature [48]
	Density of xylem (kg/m ³)	751.50	Section 2.1.2
	Shear modulus of xylem (Pa)	2.42×10^8	Section 2.1.3
Contact Parameters	Poisson's ratio of xylem	0.30	Literature [48]
	Phloem–Q235A steel coefficient of restitution	0.25	Section 2.2.1
	Phloem–Q235A steel coefficient of static friction	0.47	Section 2.2.2
	Phloem–Q235A steel coefficient of rolling friction	0.05	Section 2.2.2
	Xylem–Q235A steel coefficient of restitution	0.37	Section 2.2.1
	Xylem–Q235A steel coefficient of static friction	0.56	Section 2.2.2
	Xylem–Q235A steel coefficient of rolling friction	0.074	Section 2.2.2

3.2. Results of the Stacking Angle Measurement

The physical stacking angle images of the phloem and xylem were processed using MATLAB for grayscale processing, binarization, and extraction of the image boundary pixels. The slope of the boundary pixels was linearly fitted using the least squares method, and the angle between the stacking angle tangent and the horizontal line was defined as the stacking angle. The average of the two sides was taken as the stacking angle for the phloem, and the left degree was taken as the stacking angle value for the xylem; the image processing process is shown in Figure 10.

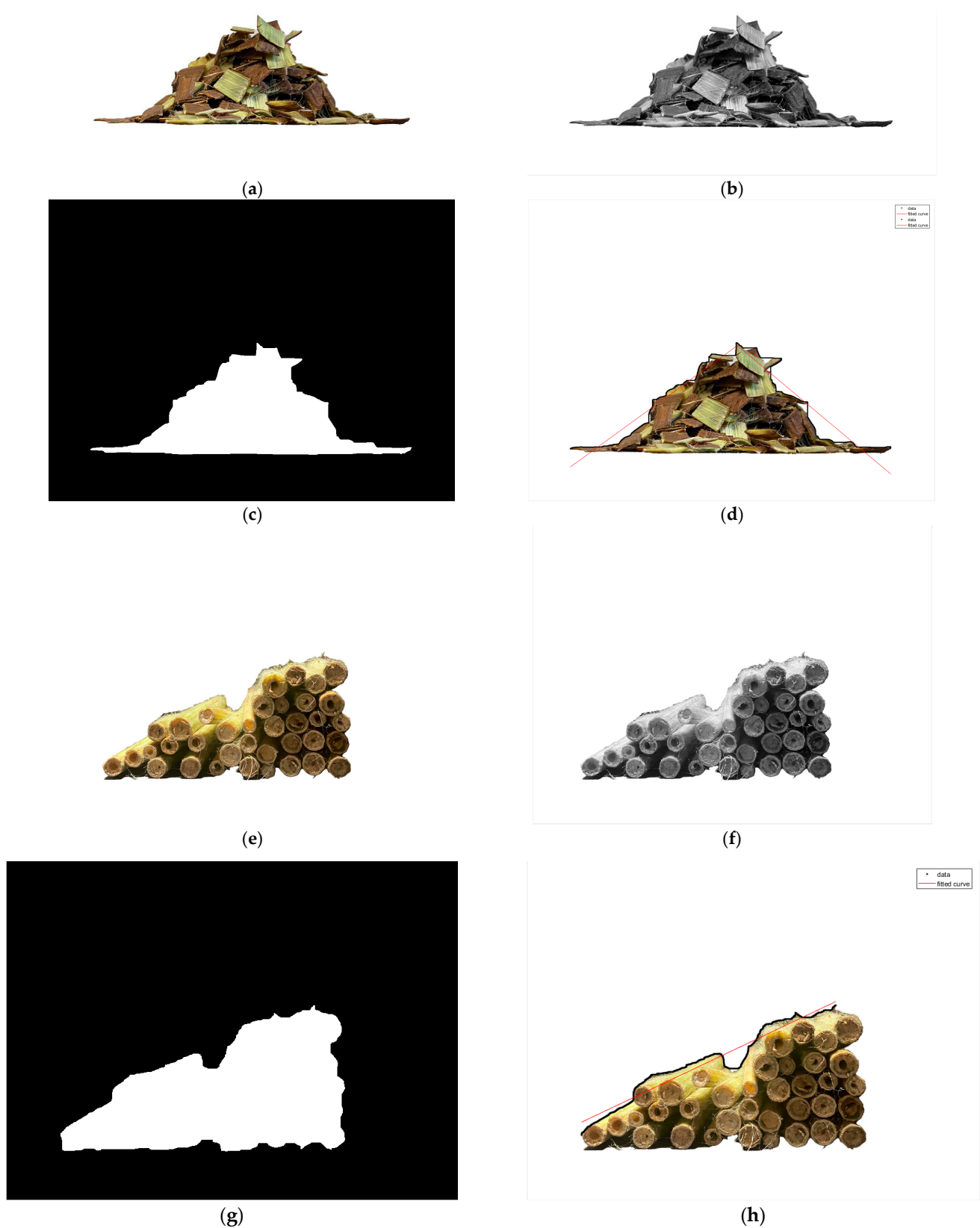


Figure 10. Physical stacking angle image processing: (a) original image of the phloem stacking angle; (b) grayscale processing of the phloem image; (c) binarization of the phloem image; (d) fitting phloem image using the least squares method; (e) original image of the xylem stacking angle; (f) grayscale processing of the xylem image; (g) binarization of the xylem image; (h) fitting xylem image using the least squares method.

The average value of the stacking angle of the xylem was determined to be 27.17° , with a standard deviation of 1.27° . The average value of the stacking angle of the phloem was 37.93° , with a standard deviation of 2.29° .

3.3. Calibration of the Contact Parameters between Phloem and Xylem

3.3.1. Phloem–Xylem Restitution Coefficient

The physical test result shows that the average maximum rebound height of the ramie xylem on the phloem was 21.3 mm. In the discrete element simulations, to avoid interference, all contact parameters, except the restitution coefficient between the xylem and phloem, were set to 0. After the presimulation tests, the restitution coefficient between the xylem and phloem ranged from 0.4 to 0.7. The simulation test design for the restitution coefficient is shown in Table 4. Three repetitions were conducted for each group, and the mean value was taken.

Table 4. Simulation test results for the restitution coefficient between xylem and phloem.

No.	Coefficient of Restitution, e_1	Maximum Bounce Height of Xylem, h_{max}/mm
1	0.40	9.46
2	0.45	11.26
3	0.50	13.67
4	0.55	16.78
5	0.60	20.80
6	0.65	26.32
7	0.7	34.91

The simulation test results in Table 4 were plotted as a scatter plot and fitted. The fitted curve obtained is shown in Figure 11. The fitting equation for the coefficient of restitution between the ramie xylem–phloem (e_1) and the maximum rebound height (h_{max}) is shown in Equation (5):

$$h_{max} = 45.91 - 187e_1 + 244.5e_1^2 \quad (5)$$

where h_{max} represents the maximum rebound height, in millimeters; e_1 represents the coefficient of restitution between the phloem and the xylem.

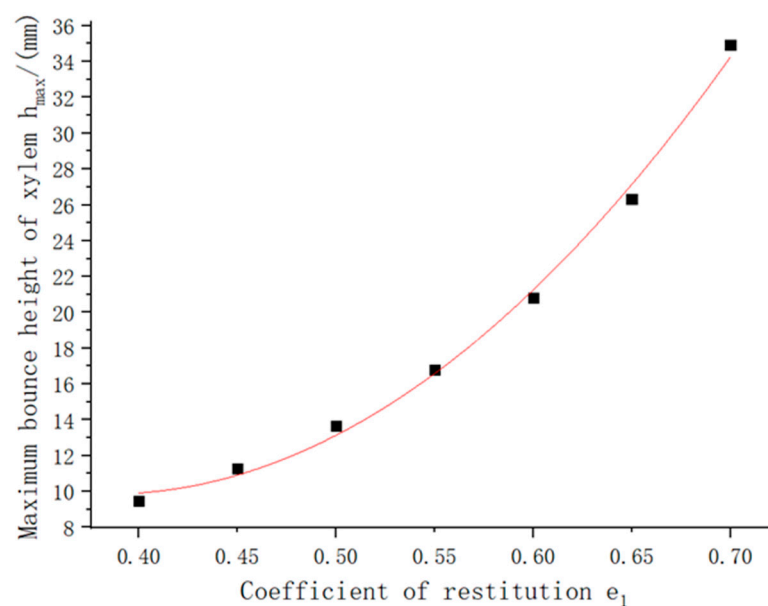


Figure 11. Fitted curve of the restitution coefficient and maximum rebound height.

The determination coefficient (R^2) of the fitting equation is 0.996, indicating the high reliability of the fitting equation. By substituting the measured maximum rebound height into Equation (5), e_1 is calculated as 0.60. Using the coefficient of restitution (e_1) for the simulation tests, repeating five times, and taking the average value, the maximum rebound height is 20.85 with an error of 2.11%. The results show that the simulation results after the calibration are consistent with the physical test results. Therefore, the coefficient of restitution between the ramie phloem and xylem was determined to be 0.60.

3.3.2. Phloem–Xylem Static Friction Coefficient

The coefficient of the static friction (μ_s) between the ramie phloem and xylem was determined by measuring the average sliding angle of the xylem on the phloem's surface during inclined plane sliding. The physical test result shows that average sliding angle between the phloem and xylem was measured to be 31.61° . In the DEM simulation test, the coefficient of restitution was set to the calibrated value, and the range of the coefficient of the static friction was set to 0.1 ~ 0.7 with an interval of 0.1. The remaining contact parameters were all set to 0. The simulation test of the static friction coefficient is shown in Table 5. Each group of tests was repeated three times, and the average value was acquired to obtain the relationship between the sliding angle and the static friction coefficient.

Table 5. Simulation test results for the static friction coefficient between the xylem and phloem.

No.	Coefficient of Static Friction, μ_s	Sliding Angle, α ($^\circ$)
1	0.10	8.43
2	0.20	14.28
3	0.30	20.75
4	0.40	25.72
5	0.50	30.19
6	0.60	34.26
7	0.70	37.93

The simulation test results were plotted as a scatter plot and fitted, and the fitting curve is shown in Figure 12. The fitting equation for the static friction coefficient between the ramie phloem–xylem (μ_s) and the sliding angle (α) is shown in Equation (6):

$$\alpha = 1.393 + 72.01\mu_s - 28.44\mu_s^2 \quad (6)$$

where α is the sliding angle in degrees, $^\circ$; and μ_s is the static friction coefficient between the phloem and xylem.

The fitting results show that the determination coefficient (R^2) of the fitting equation is 0.996, indicating that the reliability of the fitting equation is high. By substituting the measured sliding angle into Equation (6), μ_s is calculated to be 0.53. A simulated verification test was performed, and the average sliding angle was obtained by repeating the test five times, which was 31.54° . The relative error between the simulated and physical test results was 0.22%, indicating that the calibrated simulation results are consistent with the physical test results. Therefore, the coefficient of the static friction between the ramie phloem and xylem was determined to be 0.53.

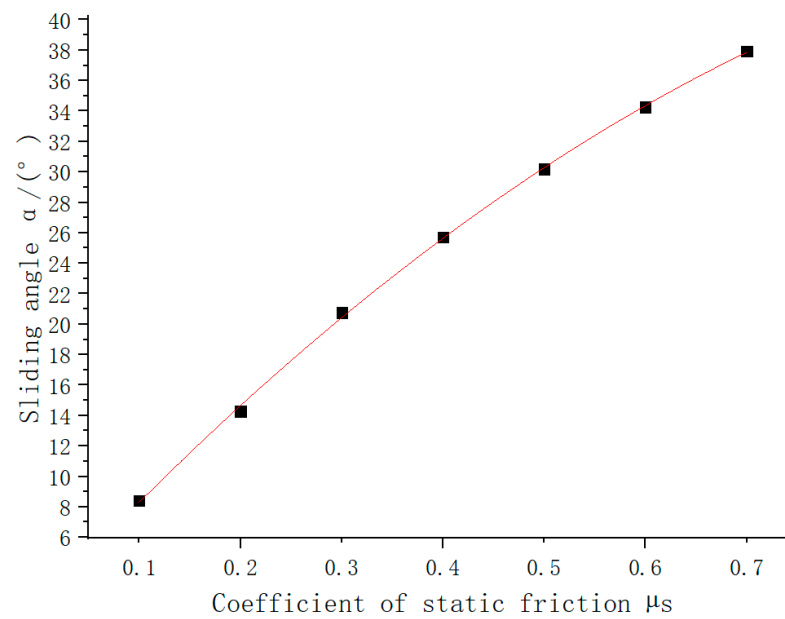


Figure 12. Fitting curve of the static friction coefficient and sliding angle.

3.3.3. Phloem–Xylem Rolling Friction Coefficient

The coefficient of the rolling friction was measured similarly to that of the coefficient of static friction. The xylem was placed radially on the surface of the phloem, and the inclined device was slowly and uniformly raised to gradually increase the phloem plate's inclination angle. When the xylem began to roll, the raising was immediately stopped, and the inclination device was fixed. The rolling angle (β) was measured and recorded by an angle display device. The test was repeated ten times, and the average rolling angle between the phloem and xylem was measured to be 3.91° .

In the DEM simulation test, the values of the restitution coefficient and static friction coefficient that had been calibrated were input. The range of the rolling friction coefficient was set to 0.01–0.04 with an interval of 0.005, and all other contact parameters were set to 0. The simulation test for the rolling friction coefficient was designed as shown in Table 6, and each group of tests was repeated three times to obtain the average value.

Table 6. Simulation test results for the rolling friction coefficient between the xylem and phloem.

No.	Coefficient of Rolling Friction, μ_r	Rolling Angle, β (°)
1	0.010	2.90
2	0.015	3.36
3	0.020	3.83
4	0.025	4.20
5	0.030	4.61
6	0.035	5.10
7	0.040	5.50

The simulation test results in Table 6 were plotted as a scatter plot and fitted, and the fitting curve is shown in Figure 13. The fitting equation for the rolling friction coefficient between the ramie phloem–xylem (μ_r) and the rolling angle (β) is provided by Equation (7):

$$\beta = 2.031 + 88.99\mu_r - 57\mu_r \quad (7)$$

where β represents the rolling angle in degrees, mm; and μ_r represents the rolling friction coefficient between the xylem and phloem.

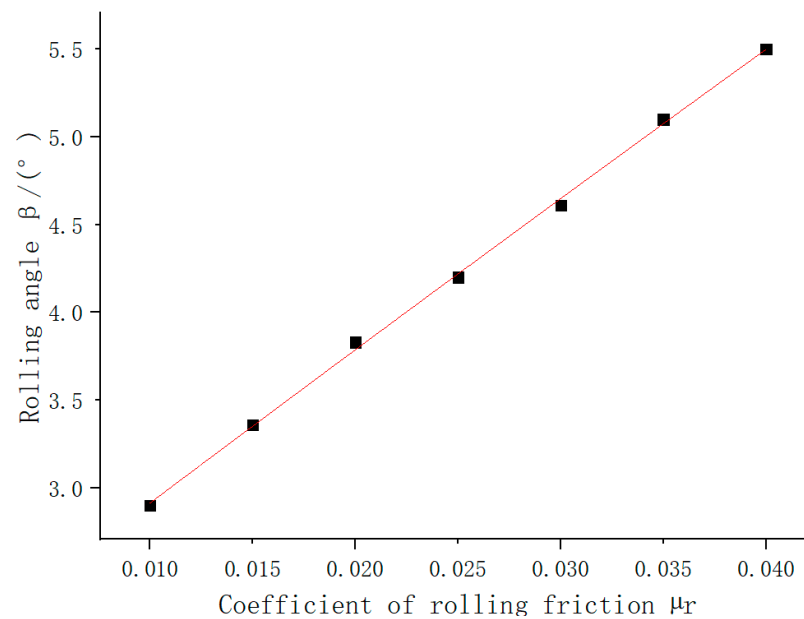


Figure 13. Fitting curve for the rolling friction coefficient and rolling angle.

The fitting result indicates that the determination coefficient (R^2) of the fitting equation is 0.999, thereby indicating a high reliability of the fitting equation. By substituting the measured rolling angle into Equation (7), μ_r was calculated to be 0.021. Through simulation verification tests conducted five times and taking the average value, the rolling angle was found to be 3.90° , with a relative error of 0.3% compared to the physical test results. This shows that the simulated test results after calibration were consistent with the physical test results, thus confirming the rolling friction coefficient between the phloem and xylem as 0.021.

Thus, the calibration of the contact parameters between the phloem and xylem of the ramie stalk by the discrete element method was completed, and the calibrated coefficients of restitution (e_1), coefficient of the static friction (μ_s), and coefficient of the rolling friction (μ_r) between the phloem and xylem were 0.60, 0.53, and 0.021, respectively.

3.4. Plackett–Burman Parameter Significance Analysis

3.4.1. Significance Analysis of Phloem Parameters

The Plackett–Burman test results for the phloem are shown in Table 7, and the Design-Expert software was used to perform a significance analysis of the results, as shown in Table 8.

Table 7. Phloem Plackett–Burman test results.

X_1	X_2	X_3	X_4	X_5	X_6	Angle ($^\circ$)
−1	−1	−1	−1	−1	−1	18.19
−1	1	1	−1	1	−1	38.94
1	−1	1	−1	−1	−1	19.40
−1	1	−1	−1	−1	1	30.67
0	0	0	0	0	0	36.35
1	1	−1	1	−1	−1	20.19
1	1	1	−1	1	1	42.99
1	−1	1	1	−1	1	30.03
1	1	−1	1	1	−1	39.12
−1	−1	−1	1	1	1	41.25
−1	−1	1	1	1	−1	38.64
−1	1	1	1	−1	1	31.28
1	−1	−1	−1	1	1	41.59

Table 8. Parameter significance analysis of the Plackett–Burman test in the phloem.

Parameters	Degree of Freedom	Sum of Squares	F-Value	p-Value	Effect Value	Significance Ranking
X ₁	1	2.67	0.59	0.5239	−0.94	6
X ₂	1	16.52	3.65	0.1433	2.35	3
X ₃	1	8.82	1.95	0.2647	1.71	4
X ₄	1	6.35	1.40	0.3370	1.45	5
X ₅	1	717.30	158.39	<0.0001	15.46	1
X ₆	1	156.46	34.55	0.0021	7.22	2

The *p*-values of the static friction coefficient between the phloem and phloem (X₅) and the rolling friction coefficient between the phloem and phloem (X₆) were less than 0.05, indicating that X₅ and X₆ have a significant effect on the stacking angle of the phloem. In contrast, the other factors have a relatively small effect. Therefore, only significant factors (i.e., X₅ and X₆) were considered for the subsequent steepest ascent test and response surface design of the phloem.

3.4.2. Significance Analysis of the Xylem Parameters

The Plackett–Burman test results for the xylem are shown in Table 9, and the Design-Expert software was used to perform a significance analysis of the results, as shown in Table 10.

Table 9. Xylem Plackett–Burman test results.

X' ₁	X' ₂	X' ₃	X' ₄	X' ₅	X' ₆	Angle (°)
1	1	1	−1	1	1	38.61
1	1	−1	1	1	−1	27.52
1	−1	1	−1	−1	−1	27.33
−1	1	1	−1	1	−1	31.96
−1	−1	−1	1	1	1	33.84
−1	−1	1	1	1	−1	32.07
1	1	−1	1	−1	−1	22.26
−1	1	1	1	−1	1	34.02
0	0	0	0	0	0	31.10
1	−1	−1	−1	1	1	33.71
−1	1	−1	−1	−1	1	30.55
−1	−1	−1	−1	−1	−1	19.65
1	−1	1	1	−1	1	34.91

Table 10. Parameter significance analysis of the Plackett–Burman test in the xylem.

Parameters	Degree of Freedom	Sum of Squares	F-Value	p-Value	Effect Value	Significance Ranking
X ₁	1	0.43	0.33	0.5620	0.38	6
X ₂	1	0.97	0.75	0.3900	0.57	4
X ₃	1	82.05	63.22	0.0001	5.23	2
X ₄	1	0.66	0.51	0.4741	0.47	5
X ₅	1	70.05	53.98	0.0002	4.83	3
X ₆	1	167.58	129.14	<0.0001	7.47	1

The results show that the *p*-values of the rolling friction coefficient between the xylem and Q235A steel (X_{3'}), the static friction coefficient between the xylem and xylem (X_{5'}), and the rolling friction coefficient between the xylem and xylem (X_{6'}) were all less than 0.05. Thus, it can be concluded that these three factors are the most critical factors affecting the stacking angle of the xylem, while other factors have relatively small effects. As a

result, only the significant factors (i.e., $X_{3'}$, $X_{5'}$, and $X_{6'}$) were considered for the subsequent steepest ascent test and response surface design of the xylem.

3.5. Results of the Steepest Ascent Test

3.5.1. Steepest Ascent Test of the Phloem

Based on the significant factors affecting the stacking angle obtained from the phloem Plackett–Burman test, the phloem–phloem static friction coefficient (X_5) and phloem–phloem rolling friction coefficient (X_6) were taken as the independent variables to carry out the steepest ascent test of the phloem. The test results are shown in Table 11. The results show that, as the values of X_5 and X_6 increased, the relative error between the simulated stacking angle and the physical stacking angle first decreased and then increased. The minimum relative error was obtained when the fifth level was selected, indicating the existence of the optimal value range for the fifth level. Therefore, the stacking angle test result of level 5 was taken as the center point, and the stacking angle test results of levels 4 and 6 were taken as the low and high levels for the subsequent response surface design. The optimization ranges of the phloem–phloem static friction coefficient (X_5) and rolling friction coefficient (X_6) were determined to be 0.35–0.52 and 0.053–0.084, respectively.

Table 11. Results of the steepest ascent test of the phloem.

No.	X_5	X_6	Stacking Angle (°)	Relative Error (%)
1	0.10	0.005	19.50	50.43
2	0.18	0.021	25.49	35.21
3	0.27	0.037	31.35	20.31
4	0.35	0.053	35.56	9.62
5	0.43	0.068	39.57	0.58
6	0.52	0.084	40.45	2.82
7	0.60	0.100	43.13	9.61

3.5.2. Steepest Ascent Test of the Xylem

Based on the Plackett–Burman test for the xylem to derive the significant influences on the stacking angle, the steepest ascent test was carried out with the xylem–Q235A steel rolling friction coefficient ($X_{3'}$), xylem–xylem static friction coefficient ($X_{5'}$), and xylem–xylem rolling friction coefficient ($X_{6'}$) as the independent variables. The test results are shown in Table 12. The results show that as the values of $X_{3'}$, $X_{5'}$, and $X_{6'}$ increased, the relative error between the simulated stacking angle and the physical stacking angle first decreased and then increased. The minimum relative error was obtained when the third level was selected, indicating the existence of the optimal value range for the third level. Therefore, the stacking angle test result of level 3 was taken as the center point, and the stacking angle test results of levels 2 and 4 were taken as the low and high levels for the subsequent response surface design. The optimization ranges of the xylem–Q235A steel rolling friction coefficient ($X_{3'}$), xylem–xylem static friction coefficient ($X_{5'}$), and xylem–xylem rolling friction coefficient ($X_{6'}$) were determined to be 0.028–0.074, 0.22–0.45, and 0.013–0.028, respectively.

Table 12. Results of the steepest ascent test of the xylem.

No.	$X_{3'}$	$X_{5'}$	$X_{6'}$	Stacking Angle (°)	Relative Error (%)
1	0.005	0.10	0.005	16.50	39.27
2	0.028	0.22	0.013	24.60	9.45
3	0.051	0.33	0.020	28.22	3.87
4	0.074	0.45	0.028	29.72	9.40
5	0.097	0.57	0.035	32.41	19.30
6	0.120	0.68	0.043	32.90	21.08
7	0.143	0.80	0.050	33.13	21.93

3.6. Response Surface Design Results

3.6.1. Regression Model Establishment and Experimental Results

Analysis of the Variance of the Regression Model in Phloem

To investigate the impact of the static friction coefficient (X_5) and rolling friction coefficient (X_6) between the ramie phloem and phloem on the phloem stacking angle (Y_1) during the response surface optimization test, we utilized the range of values obtained from the steepest ascent test. The central composite design test was then conducted using Design-Expert to optimize the response surface. Tables 13 and 14 display the factor encoding level values and central composite design experimental results, respectively. A total of thirteen parameter combinations were tested, of which five were center-level repeats.

Table 13. Factor level codes for the phloem central composite design test.

Coding	Phloem–Phloem Coefficient of Static Friction X_5	Phloem–Phloem Coefficient of Rolling Friction X_6
−1.414	0.31	0.047
−1	0.35	0.053
0	0.43	0.068
1	0.52	0.084
1.414	0.56	0.090

Table 14. The phloem central composite design test scheme and results.

No.	X_5	X_6	Stacking Angle Y_1 (°)
1	−1.414	0	35.82
2	−1	−1	35.65
3	−1	1	37.57
4	0	−1.414	37.25
5	0	0	39.69
6	0	0	39.53
7	0	0	39.51
8	0	0	39.56
9	0	0	39.55
10	0	1.414	39.78
11	1	−1	39.43
12	1	1	40.45
13	1.414	0	40.39

By employing the Design-Expert software, a second-order polynomial equation was developed through a multiple regression analysis of the central composite design experimental outcomes. The equation was used to fit the phloem stacking angle and achieve the multivariate nonlinear regression model fitting of the static friction coefficient (X_5) and rolling friction coefficient (X_6) related to the phloem stacking angle (Y_1). Furthermore, the model and coefficients were subjected to a significance test, and the regression equation is shown in Equation (8):

$$Y_1 = 39.54 + 1.64X_5 + 0.81X_6 - 0.23X_5X_6 - 0.74X_5^2 - 0.54X_6^2 \quad (8)$$

Table 15 shows the results of the variance analysis. The significance test of the regression model for the stacking angle of the ramie phloem indicated $p < 0.0001$, a lack of fit of $p = 0.1123$, a determination coefficient of 0.9976, and an adjusted determination coefficient of 0.9958. The regression model was extremely significant, the lack of fit was nonsignificant, and the model was effective. The high value of the determination coefficient (close to 1) indicates a good fit of the regression equation. The coefficient of variation was only 0.45%, and the adequate precision was 68.357, indicating a high correlation between the actual and predicted values and the high reliability of the experimental results. As shown in Table 15,

the static friction coefficient (X_5) and rolling friction coefficient (X_6) of the ramie phloem, as well as their quadratic terms (X_5^2 and X_6^2), all have an extremely significant effect on the equation. Combined with the linear regression equation, the order of the factors affecting the stacking angle is the static friction coefficient (X_5) > rolling friction coefficient (X_6) of the ramie phloem.

Table 15. ANOVA results of the phloem stacking angle.

Source	Stacking Angle Y_1 (°)				
	Sum of Squares	df	Mean Square	F-Value	p-Value
Model	32.21	5	6.44	576.29	<0.0001 **
X_5	21.53	1	21.53	1925.51	<0.0001 **
X_6	5.31	1	5.31	475.01	<0.0001 **
X_5X_6	0.20	1	0.20	18.11	0.0038 **
X_5^2	3.81	1	3.81	340.97	<0.0001 **
X_6^2	1.99	1	1.99	178.27	<0.0001 **
Residual	0.078	7	0.011		
Lack of Fit	0.058	3	0.019	3.86	0.1123
Pure Error	0.020	4	5.020×10^{-3}		
Cor Total	32.29	12			

** Indicate significance at the 0.01 level.

To visually analyze the model’s reliability, Design-Expert software’s Diagnostics module was used to obtain a quadratic model residual diagnostic plot, as shown in Figure 14. Figure 14a shows a normal plot of the residual, which can be observed to be linearly distributed on both sides of the line for each test group, indicating that the model describes the relationship between the influencing factors and phloem simulation stacking angle with sufficient reliability. Figure 14b is the residual plot of the equation and the predicted values. The random dispersion of the residuals shows an irregular distribution, indicating a good prediction of the equation. Figure 14c shows the distribution of the ratio of the predicted and experimental values of the phloem simulation stacking angle, and the linear distribution indicates a good fit of the model. Overall, these results indicate that the model’s reliability is extremely high.

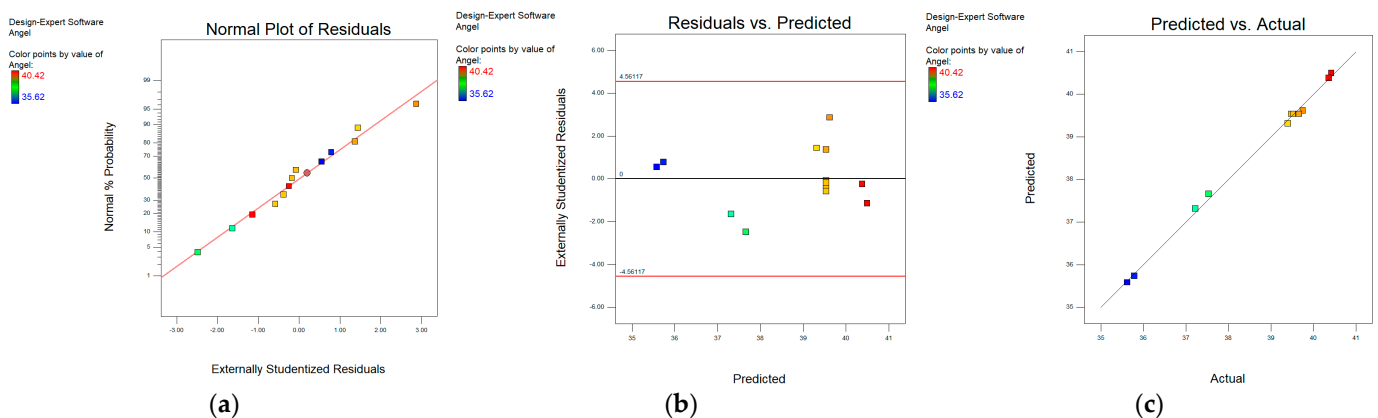


Figure 14. Diagnostic plot of the phloem quadratic model residuals: (a) normal plot; (b) residual vs. predicted; (c) predicted vs. actual.

Analysis of the Variance of the Regression Model in Xylem

Based on the interval of the values of the xylem–Q235A steel rolling friction coefficient ($X_{3'}$), xylem–xylem static friction coefficient ($X_{5'}$), and xylem–xylem rolling friction coefficient ($X_{6'}$) among the ramie xylem obtained from the steepest ascent test in order to investigate the effect of the influencing factors (i.e., $X_{3'}$, $X_{5'}$, and $X_{6'}$) on the xylem stacking

angle (Y_2) of the response surface optimization test, the central composite design test was carried out using Design-Expert. The stacking angle simulation test was conducted for 23 sets of parameter combinations of which three sets were repeated at the central level. The results of their factor coding level values and central combination tests are shown in Tables 16 and 17.

Table 16. Factor level codes for the xylem central composite design test.

Coding	Xylem–Q235A Steel Coefficient of Rolling Friction X_3	Xylem–Xylem Coefficient of Static Friction X_5	Xylem–Xylem Coefficient of Rolling Friction X_6
−1.682	0.012	0.14	0.007
−1	0.028	0.22	0.013
0	0.051	0.33	0.020
1	0.074	0.45	0.028
1.682	0.090	0.53	0.033

Table 17. The xylem central composite design test scheme and results.

No.	X_3	X_5	X_6	Stacking Angle Y_2 (°)
1	1	0	0	28.01
2	1	1	−1	27.64
3	1	1	1	29.73
4	0	0	0	27.83
5	−1	−1	1	27.11
6	0	0	0	27.81
7	1	−1	1	28.34
8	0	0	0	28.22
9	0	0	0	28.08
10	0	0	0	28.13
11	−1	1	1	27.98
12	1	−1	−1	26.05
13	−1.682	0	0	26.60
14	1.682	0	0	28.80
15	0	0	0	27.94
16	0	0	−1.682	25.32
17	−1	1	−1	26.28
18	0	1.682	0	28.40
19	0	0	0	28.16
20	0	0	1.682	29.07
21	0	0	0	28.31
22	0	−1.682	0	26.02
23	−1	−1	−1	24.62

A multivariate regression analysis was conducted on the results of the central composite design test using Design-Expert software. After eliminating the insignificant factors while ensuring the model significance and insignificance of the lack-of-fit terms, the second-order regression model was optimized to obtain a new regression equation:

$$Y_2 = 28.06 + 0.69X_3 + 0.70X_5 + 1.09X_6 - 0.12X_5X_6 - 0.15X_3^2 - 0.32X_5^2 - 0.33X_6^2 \quad (9)$$

The results of the variance analysis are shown in Table 18. The p -value ($p < 0.0001$) of the model confirms its significance within the 95% confidence interval. The p -value of the lack-of-fit term was 0.6381, less than 0.05, indicating the effectiveness of the second-order model for the xylem stacking angle. In addition, the determination coefficient and adjusted determination coefficient were 0.9899 and 0.9829, respectively, both close to 1, indicating good agreement between the calculated model and experimental data. The difference between the adjusted determination coefficient and the predictive determination coefficient

of 0.9657 was less than 0.2, indicating a good fit, and the adequate precision was 46.594, indicating a high correlation between the actual and predicted values.

Table 18. ANOVA results of the xylem stacking angle.

Source	Stacking Angle Y_2 (°)				
	Sum of Squares	df	Mean Square	F-Value	p-Value
Model	33.18	9	3.69	141.54	<0.0001 **
X_3	6.57	1	6.57	252.10	<0.0001 **
X_5	6.63	1	6.63	254.38	<0.0001 **
X_6	16.21	1	16.21	622.14	<0.0001 **
X_3X_5	0.025	1	0.025	0.97	0.3422
X_3X_6	4.512×10^{-3}	1	4.512×10^{-3}	0.17	0.6840
X_5X_6	0.12	1	0.12	4.70	0.0492 *
X_3^2	0.35	1	0.35	13.34	0.0029 **
X_5^2	1.64	1	1.64	62.83	<0.0001 **
X_6^2	1.69	1	1.69	64.93	<0.0001 **
Residual	0.34	13	0.026		
Lack of Fit	0.10	5	0.021	0.70	0.6381
Pure Error	0.24	8	0.029		
Cor Total	33.52	22			

** , * Indicate significance at the 0.01 and 0.05 levels, respectively.

Based on the Diagnostics module in the Design-Expert software, the residual diagnostic plots of the quadratic model were obtained, as shown in Figure 15. Figure 15a shows a normal plot of the residual, which can be observed to be linearly distributed on both sides of the line for each test group, indicating that the model describes the relationship between the influencing factors and the xylem simulation stacking angle with sufficient reliability. Figure 15b is the residual plot of the equation and the predicted values. The random dispersion of the residuals shows an irregular distribution, indicating a good prediction of the equation. Figure 15c shows the distribution of the ratio of the predicted and experimental values of the xylem simulation stacking angle. The linear distribution indicates a good fit for the model. Overall, these results suggest that the model’s reliability is extremely high.

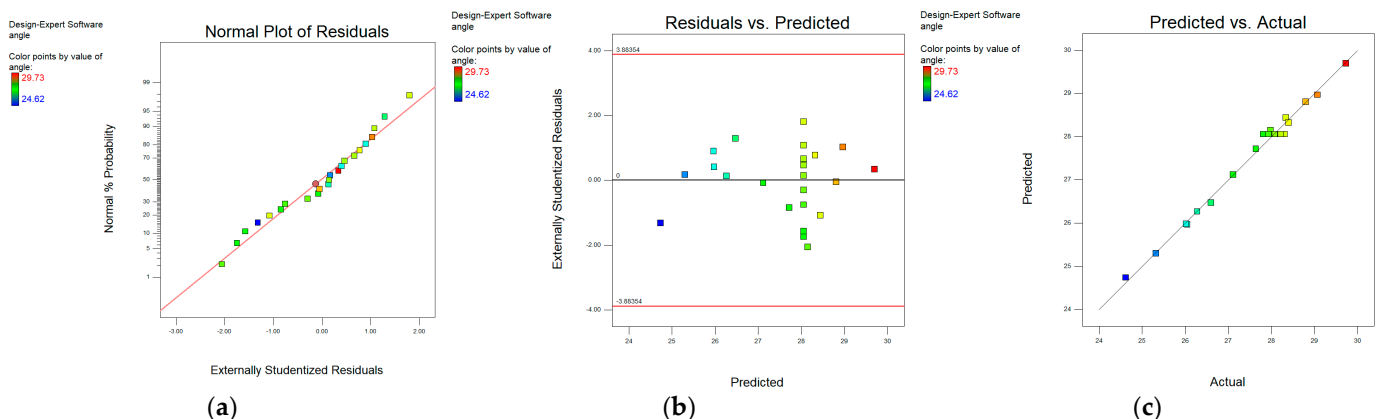


Figure 15. Diagnostic plot of the xylem quadratic model residuals: (a) normal plot; (b) residual vs. predicted; (c) predicted vs. actual.

3.6.2. Analysis of the Interaction Effects among the Factors

Interaction Effects of the Factors in the Phloem on the Simulation Stacking Angle

Based on the variance analysis of the phloem simulation stacking angle, the static friction coefficient (X_5) and rolling friction coefficient (X_6) between the phloem and phloem

had an extremely significant impact on the phloem simulation stacking angle. Therefore, the Design-Expert software was used to analyze the nonlinear relationship between X_5 , X_6 , and the phloem simulation stacking angle. Figure 16 shows the response surface of the interaction between X_5 and X_6 on the phloem simulation stacking angle. When the static friction coefficient among the phloem was constant, the phloem simulation stacking angle increased with the rise in the rolling friction coefficient between the phloem and phloem. When the rolling friction coefficient between the phloem and phloem was constant, the phloem simulation stacking angle increased with the rise in the static friction coefficient between the phloem and phloem. However, the contour slope of X_5 was steeper than X_6 , indicating that the static friction coefficient between the phloem and phloem (X_5) had a more significant impact on the phloem simulation stacking angle than the rolling friction coefficient between the phloem and phloem (X_6). Therefore, the order of the effects of each factor on the phloem simulation stacking angle is $X_5 > X_6$, which is consistent with the results of the variance analysis.

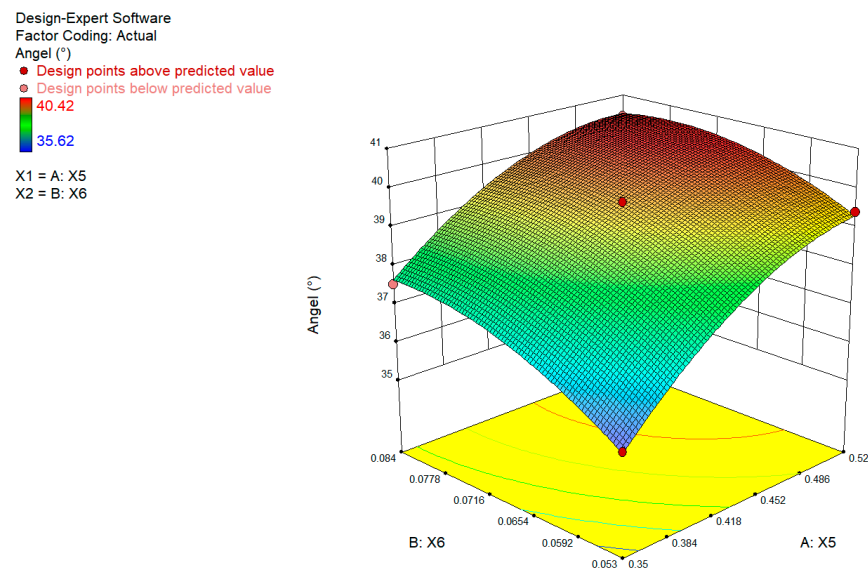


Figure 16. Response surface of the interaction effects of the factors in the phloem on the stacking angle.

Interaction Effects of the Factors in the Xylem on the Simulation Stacking Angle

Based on the analysis of the variance of the xylem simulation stacking angle ($X_3^{2'}$, $X_5^{2'}$ and $X_6^{2'}$) had an extremely significant impact on the simulation stacking angle. $X_5^{2'}$ and $X_6^{2'}$ significantly affected the simulation stacking angle, while $X_3^{2'}$ and $X_5^{2'}$ and $X_3^{2'}$ and $X_6^{2'}$ had no significant effect on the simulation stacking angle. Therefore, Design-Expert software was used to analyze the relationship between the static friction coefficient ($X_5^{2'}$), rolling friction coefficient ($X_6^{2'}$), and xylem and the xylem simulation stacking angle. Figure 17 shows the response surface of the interaction between $X_5^{2'}$ and $X_6^{2'}$ on the simulation stacking angle. When $X_5^{2'}$ was constant, the simulation stacking angle increased with the increase in $X_6^{2'}$. When $X_6^{2'}$ was constant, the simulation stacking angle increased with the rise in $X_5^{2'}$. However, the contour slope of $X_6^{2'}$ was steeper than that of $X_5^{2'}$, indicating that $X_6^{2'}$ had a more significant impact on the simulation stacking angle. Therefore, the order of the effects of each factor on the simulation stacking angle is $X_6^{2'} > X_5^{2'} > X_3^{2'}$, which is consistent with the results of the variance analysis.

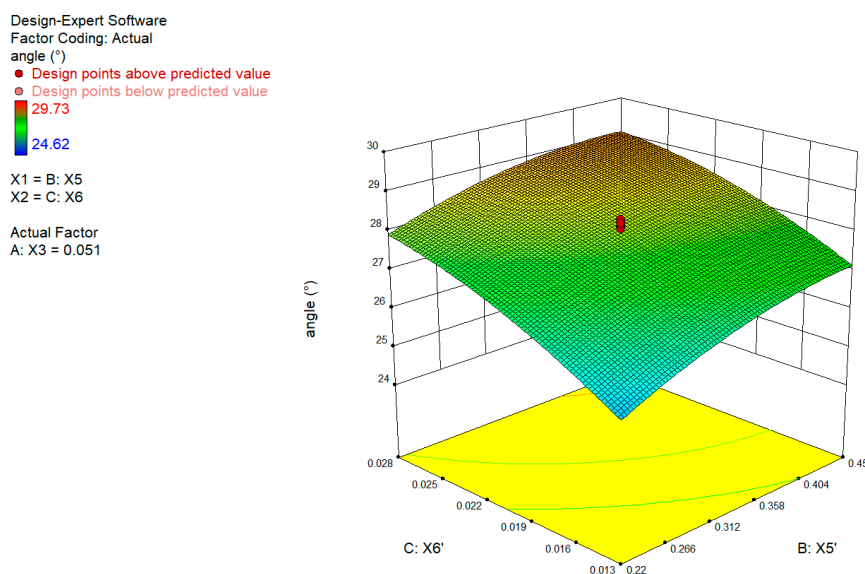


Figure 17. Response surface of the interaction effects of the factors in the xylem on the stacking angle.

3.6.3. Parameter Optimization and Validation

Optimization of the Parameters in the Phloem

Based on the results of the Plackett–Burman test and the steepest ascent test in the phloem, the ranges of X_5 and X_6 were 0.35–0.52 and 0.053–0.084, respectively. Taking the physical test value of the stacking angle of the phloem as the optimization objective, using the parameter Optimization module built into the Design-expert software, the non-significant factors were taken as the physical test values, and the rest were taken as the middle values of the steepest ascent test level to determine the optimal combination of the static friction coefficient (X_5) and rolling friction coefficient (X_6) of the phloem–phloem; the optimization objective function and constraints are shown in Equation (10):

$$\begin{cases} \text{tar}Y_1 = 37.93 \\ 0.35 \leq X_5 \leq 0.52 \\ 0.053 \leq X_6 \leq 0.084 \end{cases} \quad (10)$$

After solving, 44 sets of optimized solutions were obtained. The simulated results of the optimized parameter group were compared with the physical test results. The optimized solution with the most similar shape of the cylindrical lifting physical test stacking angle was found. The static friction coefficient (X_5) between the phloem and phloem particles was determined to be 0.41, and the rolling friction coefficient (X_6) between the phloem and phloem particles was 0.056.

Optimization of the Parameters in the Xylem

Based on the results of the xylem Plackett–Burman and steepest ascent test, the ranges of $X_{3'}$, $X_{5'}$, and $X_{6'}$ were 0.028–0.074, 0.22–0.45, and 0.013–0.028, respectively. Taking the physical test value of the xylem stacking angle as the optimization objective, using the parameter Optimization module built into the Design-expert software, the nonsignificant factors were taken as the physics test values, and the rest were taken as the middle values of the steepest ascent test level to determine the optimal combination of the xylem–Q235A steel rolling friction coefficient ($X_{3'}$), static friction coefficient ($X_{5'}$) of the xylem–xylem, and

rolling friction coefficient ($X_{6'}$) of the xylem–xylem; the optimization objective function and constraints are shown in Equation (11):

$$\begin{cases} \text{tar}Y_2 = 27.17 \\ 0.028 \leq X_{3'} \leq 0.074 \\ 0.22 \leq X_{5'} \leq 0.45 \\ 0.013 \leq X_{6'} \leq 0.028 \end{cases} \quad (11)$$

After solving, 100 sets of optimized solutions were obtained. The simulated results of the optimized parameter group were compared with the physical test results. The optimized solution with the most similar shape of the xylem stacking physical test angle was found. The rolling friction coefficient ($X_{3'}$) between the xylem and Q235A steel was determined to be 0.033, the static friction coefficient ($X_{5'}$) between the xylem and xylem was 0.44, and the rolling friction coefficient ($X_{6'}$) between the xylem and xylem was 0.016.

Determination and Validation of the Optimal Parameter Combination

The optimized solutions for the phloem were subjected to simulation tests, and the simulated stacking angles were 38.23°, 38.06°, 37.84°, 37.93°, and 38.12°. The simulated results were close to the cylindrical lifting physical test angle, as shown in Figure 18, with relative errors of 0.79%, 0.34%, 0.24%, 0.11%, and 0.5%, respectively.

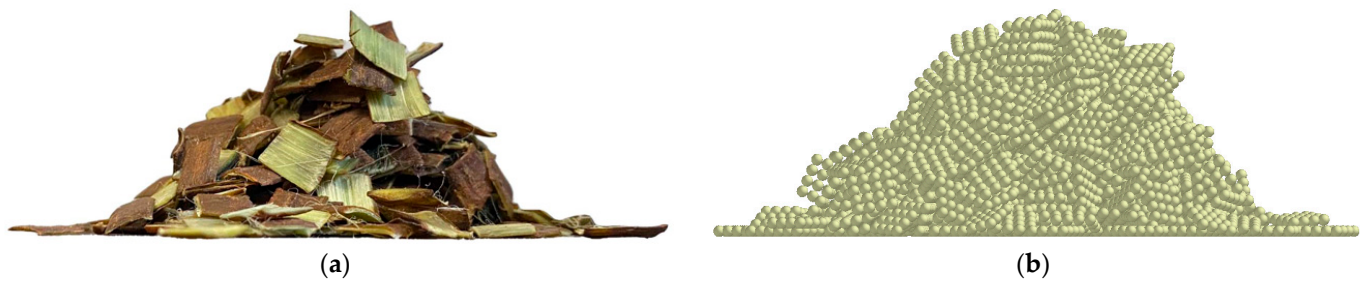


Figure 18. Comparison of the physical test and simulation test of the ramie phloem stacking angle: (a) physical test; (b) simulation test.

To evaluate the difference between the simulation and physical results of the phloem stacking angles, a two-sample *t*-test was conducted. Before conducting the two-sample *t*-test, the existence of significant differences in the variance between the two samples needed to be determined. Therefore, an *F*-test was conducted on the physical stacking angle results to test the simulation results. Table 19 shows the *F*-test results of the phloem.

Table 19. Results of the phloem *F*-test.

	Mean (°)	Variance	Observed Value	df	<i>F</i>	<i>p</i> (<i>F</i> ≤ <i>f</i>) One-Tailed	<i>F</i> One-Tailed Critical
Simulated value	38.04	0.0219	5	4	0.0041	5.1495 × 10 ^{−5}	0.1565
Physical value	37.93	5.2639	5	4			

The phloem samples showed a significant difference between the two variances, with a two-tailed probability of $2p < 0.01$. Therefore, a two-sample heteroskedasticity *t*-test was conducted to assess the significance between the simulation and physical results. Table 20 displays the results of the two-sample heteroskedasticity *t*-test of the phloem.

Table 20. Results of the phloem two-sample heteroskedasticity *t*-test.

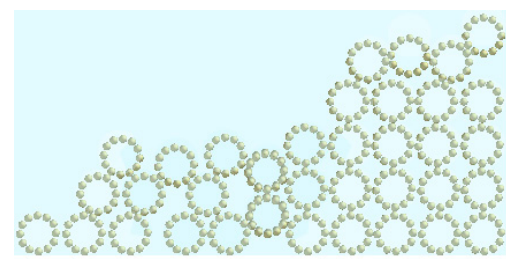
	Mean (°)	Variance	Observed Value	Assume Average Difference	df	<i>t</i> Stat	<i>p</i> ($T \leq t$) One-Tailed	<i>t</i> One-Tailed Critical	<i>p</i> ($T \leq t$) Two-Tailed	<i>t</i> Two-Tailed Critical
Simulated value	38.04	0.02193	5	0	4	0.1120	0.4581	2.1318	0.9162	2.7764
Physical value	37.93	5.2639	5							

According to Table 20, $|t| < "t \text{ two-tailed critical}"$ and " $p \text{ two-tailed critical} > 0.05$ ", indicating that there was no significant difference between the phloem simulation and physical results after calibrating the simulation parameters.

The simulated accumulation angles of the xylem were 27.13°, 27.3°, 27.38°, 27.05°, and 27.12°. The simulated results were close to the physical results, as shown in Figure 19, with relative errors of 0.15%, 0.48%, 0.77%, 0.44%, and 0.18%, respectively.



(a)



(b)

Figure 19. Comparison of the physical test and simulation test of the ramie xylem stacking angle: (a) physical test; (b) simulation test.

To evaluate the difference between the simulation and physical results of the xylem stacking angles, a two-sample *t*-test was conducted. Before performing the two-sample *t*-test, it was important to assess the variance between the two samples to determine if there was a significant difference. Therefore, an *F*-test was performed on the simulation results based on the physical stacking angle results, and Table 21 shows the *F*-test results for the xylem.

Table 21. Results of the xylem *F*-test.

	Mean (°)	Variance	Observed Value	df	<i>F</i>	<i>p</i> ($F \leq f$) One-Tailed	<i>F</i> One-Tailed Critical
Simulated value	27.20	0.0190	5	4	0.0119	0.0004	0.1565
Physical value	27.17	1.6004	5	4			

The xylem samples showed a significant difference between the two variances, with a two-tailed probability of $2p < 0.01$. Therefore, a two-sample heteroskedasticity *t*-test was conducted to assess the significance between the simulation and physical results. Table 22 displays the results of the two-sample heteroskedasticity *t*-test of the xylem.

According to Table 22, $|t| < "t \text{ two-tailed critical}"$ value and " $p \text{ two-tailed} > 0.05$ ", indicating no significant difference between the xylem simulated and physical results after calibrating the simulation parameters.

Table 22. Results of the xylem two-sample heteroskedasticity *t*-test.

	Mean (°)	Variance	Observed Value	Assume Average Difference	df	<i>t</i> Stat	<i>p</i> ($T \leq t$) One-Tailed	<i>t</i> One-Tailed Critical	<i>p</i> ($T \leq t$) Two-Tailed	<i>t</i> Two-Tailed Critical
Simulated value	27.20	0.0190	5	0	4	0.0459	0.4828	2.1318	0.9656	2.7764
Physical value	27.17	1.6004	5							

The results show that after optimizing the simulation parameters, the optimal parameter combination for the stacking angle simulation test and the physical test was when: the static friction coefficient (X_5) between the phloem and phloem was 0.41; rolling friction coefficient between the phloem and phloem (X_6) was 0.056; rolling friction coefficient ($X_{3'}$) between the xylem and Q235A steel was 0.033; the static friction coefficient ($X_{5'}$) between the xylem and xylem was 0.44; and rolling friction coefficient ($X_{6'}$) between the xylem and xylem was 0.016. There was no significant difference between the stacking angle simulation test results and the physical test results. The similarity in the shape and result of the stacking angle between the two indicates that the simulation parameters were accurately set. In addition, the maximum relative error between the simulated and physical results for the phloem was 0.79%, and for the xylem it was 0.77%. The average relative error between the two was only 0.4%. This further verifies the reliability and authenticity of the simulation test. The obtained parameters can be used for subsequent simulation tests on calibrating the ramie stalk's bonding parameters and the ramie stalk's discrete element decorticating simulation test.

4. Conclusions

- (1) By comparing the results of the physical and simulation tests, the contact parameters between the ramie stalk phloem and xylem were calibrated. The coefficient of restitution between the ramie stalk phloem and xylem was calibrated to 0.60 by the collision rebound test. The coefficient of the static friction between the ramie stalk phloem and xylem was calibrated to be 0.53 using the sliding test. The coefficient of the rolling friction between the ramie stalk phloem and xylem was calibrated to be 0.021 using the beveled rolling test. The calibration errors of the parameters were 2.11%, 0.22%, and 0.3%, respectively. The results indicate that the calibration results of the contact parameters between the ramie stalk phloem and xylem are reliable.
- (2) By using the Plackett–Burman and steepest ascent tests, the significant factors that influence the stacking angle of the ramie stalk phloem and xylem were screened, and their ranges were determined. The Plackett–Burman test results showed that the static friction coefficient (X_5) and rolling friction coefficient (X_6) between the phloem and phloem had a significant influence on the stacking angle of the phloem, while the rolling friction coefficient ($X_{3'}$) between the xylem and Q235A steel, static friction coefficient ($X_{5'}$), and the rolling friction coefficient ($X_{6'}$) between the xylem and xylem had a significant influence on the stacking angle of the xylem. The results of the steepest ascent test showed that the optimized ranges of the static friction coefficient (X_5) and rolling friction coefficient (X_6) between the phloem and phloem were 0.35–0.52 and 0.053–0.084, respectively, and the optimized ranges of the rolling friction coefficient ($X_{3'}$) between the xylem and Q235A steel, static friction coefficient ($X_{5'}$), and rolling friction coefficient ($X_{6'}$) between the xylem and xylem were 0.028–0.074, 0.22–0.45, and 0.013–0.028, respectively.
- (3) Using the response surface methodology, the interaction effects of the various factors in the phloem and xylem on the stacking angle were analyzed. Based on the results of the phloem central composite design test, a regression model was established between the static friction coefficient (X_5) and rolling friction coefficient (X_6) of the phloem–phloem and the stacking angle of the phloem. The results indicate that when the static

friction coefficient (X_5) between the phloem and phloem was constant, the phloem simulation stacking angle increased with the rise in the rolling friction coefficient of the phloem–phloem. When the rolling friction coefficient (X_6) of the phloem–phloem was constant, the phloem simulation stacking angle increased with the rise in the static friction coefficient (X_5) between the phloem and phloem. Factor X_5 had a more significant effect on the stacking angle than X_6 . Based on the results of the xylem central composite design test, a regression model was established between the rolling friction coefficient ($X_{3'}$) of the xylem-Q235A steel, the static friction coefficient ($X_{5'}$) of the xylem–xylem, and the rolling friction coefficient ($X_{6'}$) of the xylem–xylem and the stacking angle of the xylem. The results indicated that the order of the influence of each factor on the stacking angle is $X_{6'} > X_{5'} > X_{3'}$.

- (4) Utilizing the Optimization module in the Design-Expert software, the optimal parameters for the significant factors of the phloem, xylem, and stacking angle were obtained. Specifically, the static friction coefficient (X_5) between the phloem and phloem was 0.41, and the rolling friction coefficient (X_6) between the phloem and phloem was 0.056. The rolling friction coefficient ($X_{3'}$) between the xylem and Q235A steel was 0.033, the static friction coefficient ($X_{5'}$) between the xylem and xylem was 0.44, and the rolling friction coefficient ($X_{6'}$) between the xylem and xylem was 0.016. A two-sample heteroscedastic t -test was performed on the optimized simulation parameter results and the physical stacking angle measurement results. The results showed no significant difference between the simulated and physical values, with a maximum relative error of 0.79% for the phloem and 0.77% for the xylem, and an average relative error of only 0.4%. This verified the reliability and authenticity of the simulation test, which can provide technical support for subsequent simulation tests on ramie stalk bonding parameters to optimize ramie decorticating machines.

Author Contributions: Conceptualization, Y.H. and W.X.; methodology, Y.H. and W.X.; software, Y.H. and Y.D.; validation, Y.H. and L.M.; formal analysis, Y.H. and W.X.; investigation, Y.H. and W.X.; resources, J.L. (Jiangnan Lyu); data curation, J.L. (Jiangnan Lyu) and J.L. (Jiajie Liu); writing—original draft preparation, Y.H. and W.X.; writing—review and editing, W.X. and J.L. (Jiangnan Lyu); visualization, J.L. (Jiangnan Lyu) and B.Y.; supervision, W.X., L.M. and J.L. (Jiajie Liu); project administration, J.L. (Jiangnan Lyu) and W.X.; funding acquisition, J.L. (Jiangnan Lyu) All authors have read and agreed to the published version of the manuscript.

Funding: This research was funded by the CARS—Bast Fiber Crops (No. CARS-16-E21) and the Natural Science Foundation of Hunan Province (No. 2019JJ40333).

Institutional Review Board Statement: Not applicable.

Informed Consent Statement: Not applicable.

Data Availability Statement: All data are presented in this article in the form of figures and tables.

Conflicts of Interest: The authors declare no conflict of interest.

References

- Cheng, L.; Duan, S.; Feng, X.; Zheng, K.; Yang, Q.; Xu, H.; Luo, W.; Peng, Y. Ramie-degumming methodologies: A short review. *J. Eng. Fibers Fabr.* **2020**, *15*, 1558925020940105. [[CrossRef](#)]
- Zhu, T.; Zhu, A.; Yu, Y.; Sun, K.; Mao, H.; Chen, Q. Research progress of ramie for feedstuff. *Pratac. Sci.* **2016**, *33*, 338–347.
- Pandey, S. Ramie fibre: Part II. Physical fibre properties. A critical appreciation of recent developments. *Text. Prog.* **2007**, *39*, 189–268. [[CrossRef](#)]
- Du, X.; Zhao, W.; Wang, Y.; Wang, C.; Chen, M.; Qi, T.; Hua, C.; Ma, M. Preparation of activated carbon hollow fibers from ramie at low temperature for electric double-layer capacitor applications. *Bioresour. Technol.* **2013**, *149*, 31–37. [[CrossRef](#)] [[PubMed](#)]
- Rehman, M.; Gang, D.; Liu, Q.; Chen, Y.; Wang, B.; Peng, D.; Liu, L. Ramie, a multipurpose crop: Potential applications, constraints and improvement strategies. *Ind. Crops Prod.* **2019**, *137*, 300–307. [[CrossRef](#)]
- Xiang, W.; Ma, L.; Liu, J.; Xiao, L.; Long, C.; Wen, Q.; Lyu, J. Research progress on technology and equipment of ramie fibre stripping and processing in China. *J. Agric. Sci. Technol.* **2019**, *21*, 59–69.
- Lyu, J.; Long, C.; Zhao, J.; Ma, L.; Lyu, H.; Liu, J.; He, H. Design and experiment of transverse-feeding ramie decorticator. *Trans. Chin. Soc. Agric. Eng.* **2013**, *29*, 16–21.

8. Yan, D.; Yu, J.; Wang, Y.; Zhou, L.; Sun, K.; Tian, Y. A review of the application of discrete element method in agricultural engineering: A case study of soybean. *Processes* **2022**, *10*, 1305. [[CrossRef](#)]
9. Zeng, Z.; Ma, X.; Cao, X.; Li, Z.; Wang, X. Critical review of applications of discrete element method in agricultural engineering. *Trans. Chin. Soc. Agric. Mach.* **2021**, *52*, 1–20.
10. Shi, L.; Zhao, W.; Sun, B.; Sun, W. Determination of the coefficient of rolling friction of irregularly shaped maize particles by using discrete element method. *Int. J. Agric. Biol. Eng.* **2020**, *13*, 15–25. [[CrossRef](#)]
11. Zhao, H.; Huang, Y.; Liu, Z.; Liu, W.; Zheng, Z. Applications of discrete element method in the research of agricultural machinery: A review. *Agriculture* **2021**, *11*, 425. [[CrossRef](#)]
12. Ma, H.; Zhou, L.; Liu, Z.; Chen, M.; Xia, X.; Zhao, Y. A review of recent development for the CFD-DEM investigations of non-spherical particles. *Powder Technol.* **2022**, *412*, 117972. [[CrossRef](#)]
13. Roessler, T.; Richter, C.; Katterfeld, A.; Will, F. Development of a standard calibration procedure for the DEM parameters of cohesionless bulk materials—Part I: Solving the problem of ambiguous parameter combinations. *Powder Technol.* **2019**, *343*, 803–812. [[CrossRef](#)]
14. Elskamp, F.; Kruggel-Emden, H.; Hennig, M.; Teipel, U. A strategy to determine DEM parameters for spherical and non-spherical particles. *Granul. Matter* **2017**, *19*, 46. [[CrossRef](#)]
15. Al-Hashemi, H.M.B.; Al-Amoudi, O.S.B. A review on the angle of repose of granular materials. *Powder Technol.* **2018**, *330*, 397–417. [[CrossRef](#)]
16. Jiang, W.; Wang, L.; Tang, J.; Yin, Y.; Zhang, H.; Jia, T.; Qin, J.; Wang, H.; Wei, Q. Calibration and experimental validation of contact parameters in a discrete element model for tobacco strips. *Processes* **2022**, *10*, 998. [[CrossRef](#)]
17. Zhang, T.; Liu, F.; Zhao, M.; Ma, Q.; Wang, W.; Fan, Q.; Yan, P. Determination of corn stalk contact parameters and calibration of Discrete Element Method simulation. *J. China Agric. Univ.* **2018**, *23*, 120–127.
18. Xiang, W.; Wu, M.; Lu, J.; Quan, W.; Ma, L.; Liu, J. Calibration of simulation physical parameters of clay loam based on soil accumulation test. *Trans. Chin. Soc. Agric. Eng.* **2019**, *35*, 116–123.
19. Liu, F.; Zhang, J.; Li, B.; Chen, J. Calibration of parameters of wheat required in discrete element method simulation based on repose angle of particle heap. *Trans. Chin. Soc. Agric. Eng.* **2016**, *32*, 247–253.
20. Xiao, W.; Chen, H.; Wan, X.; Li, M.; Liao, Q. Influence of shape and particle size distribution on discrete element simulation flow characteristics of granular compound fertilizers. *Appl. Eng. Agric.* **2021**, *37*, 1169–1179. [[CrossRef](#)]
21. Shi, G.; Li, J.; Ding, L.; Zhang, Z.; Ding, H.; Li, N.; Kan, Z. Calibration and tests for the discrete element simulation parameters of fallen jujube fruit. *Agriculture* **2022**, *12*, 38. [[CrossRef](#)]
22. Dai, Z.; Wu, M.; Fang, Z.; Qu, Y. Calibration and verification test of lily bulb simulation parameters based on discrete element method. *Appl. Sci.* **2021**, *11*, 10749. [[CrossRef](#)]
23. Gupta, M.; Yang, J.; Roy, C. Density of softwood bark and softwood char: Procedural calibration and measurement by water soaking and kerosene immersion method. *Fuel* **2002**, *81*, 1379–1384. [[CrossRef](#)]
24. GB/T 1931-2009; Method for Determination of the Moisture Content of Wood. Standardization Administration of the P.R.C.: Beijing, China, 2009.
25. Navi, P.; Rastogi, P.K.; Gresse, V.; Tolou, A. Micromechanics of wood subjected to axial tension. *Wood Sci. Technol.* **1995**, *29*, 411–429. [[CrossRef](#)]
26. Du, D.; Wang, J. Research on mechanics properties of crop stalks: A review. *Int. J. Agric. Biol. Eng.* **2016**, *9*, 10–19.
27. Xie, H.; Cui, B.; Hao, S.; Li, S.; Jia, X.; Wang, W. Exploring the macroscopic and microscopic characteristics of rice stalk for utilization in bio-composites. *Compos. Sci. Technol.* **2022**, *230*, 109728. [[CrossRef](#)]
28. Liu, P.; Xiang, P.; Zhou, Q.; Zhang, H.; Tian, J.; Argaw, M.D. Prediction of Mechanical Properties of Structural Bamboo and Its Relationship with Growth Parameters. *J. Renew. Mater.* **2021**, *9*, 2223–2239. [[CrossRef](#)]
29. Tian, K.P.; Shen, C.; Zhang, B.; Li, X.W.; Huang, J.C.; Chen, Q.M. Experimental study on mechanical properties of reed stalk. *IOP Conf. Ser. Earth Environ. Sci.* **2019**, *346*, 012076. [[CrossRef](#)]
30. Al-Zube, L.; Sun, W.; Robertson, D.; Cook, D. The elastic modulus for maize stems. *Plant Methods* **2018**, *14*, 1–12. [[CrossRef](#)]
31. GB/T 1929-2009; Method for Sample Logs Sawing and Test Specimens Selection for Physical and Mechanical Tests of Wood. Standardization Administration of the P.R.C.: Beijing, China, 2009.
32. Guo, Y.; Liang, L.; Zhang, J. *Research on Mechanical Properties of Stalk Crops and Physical Properties of Lemon Sticks and Their Applications*, 1st ed.; Chemical Industry Press: Beijing, China, 2019; pp. 111–118.
33. Sharma, R.K.; Bilanski, W.K. Coefficient of restitution of grains. *Trans. Am. Soc. Agric. Eng.* **1971**, *14*, 216–218.
34. Ma, Y.; Zhang, J.; Wu, Y. *Agricultural Material Science*, 1st ed.; Chemical Industry Press: Beijing, China, 2015; pp. 87–92.
35. Jia, H.; Deng, J.; Deng, Y.; Chen, T.; Wang, G.; Sun, Z.; Guo, H. Contact parameter analysis and calibration in discrete element simulation of rice straw. *Int. J. Agric. Biol. Eng.* **2021**, *14*, 72–81. [[CrossRef](#)]
36. ASTM G194-08; Standard Test Method for Measuring Rolling Friction Characteristics of a Spherical Shape on a Flat Horizontal Plane. ASTM International: West Conshohocken, PA, USA, 2009.
37. Wolf, D.E. *Friction in Granular Media*; NATO Advanced Study Institute on Physics of Dry Granular Media: Cargese, France, 1997; pp. 441–464.
38. Wen, X.; Yang, W.; Guo, W.; Zeng, B. Parameter determination and validation of discrete element model of segmented sugarcane harvester for impurity removal. *J. Chin. Agric. Mech.* **2020**, *41*, 12–18.

39. Zhao, L.; Zhou, H.; Xu, L.; Song, S.; Zhang, C.; Yu, Q. Parameter calibration of coconut bran substrate simulation model based on discrete element and response surface methodology. *Powder Technol.* **2022**, *395*, 183–194. [[CrossRef](#)]
40. Ren, J.; Wu, T.; Mo, W.; Li, K.; Hu, P.; Xu, F.; Liu, Q. Discrete element simulation modeling method and parameters calibration of sugarcane leaves. *Agronomy* **2022**, *12*, 1796. [[CrossRef](#)]
41. Liu, F.; Zhang, J.; Chen, J. Modeling of flexible wheat straw by discrete element method and its parameters calibration. *Int. J. Agric. Biol. Eng.* **2018**, *11*, 42–46. [[CrossRef](#)]
42. Liao, Y.; Liao, Q.; Zhou, Y.; Wang, Z.; Jiang, Y.; Liang, F. Parameters calibration of discrete element model of fodder rape crop harvest in bolting stage. *Trans. Chin. Soc. Agric. Mach.* **2020**, *51*, 73–82.
43. Zeng, Z.; Chen, Y. Simulation of straw movement by discrete element modelling of straw-sweep-soil interaction. *Biosyst. Eng.* **2019**, *180*, 25–35. [[CrossRef](#)]
44. Fan, G.; Wang, S.; Shi, W.; Gong, Z.; Gao, M. Simulation parameter calibration and test of typical pear varieties based on discrete element method. *Agronomy* **2022**, *12*, 1720. [[CrossRef](#)]
45. Cabiscol, R.; Finke, J.H.; Kwade, A. Calibration and interpretation of DEM parameters for simulations of cylindrical tablets with multi-sphere approach. *Powder Technol.* **2018**, *327*, 232–245. [[CrossRef](#)]
46. Kruggel-Emden, H.; Rickelt, S.; Wirtz, S.; Scherer, V. A study on the validity of the multi-sphere discrete element method. *Powder Technol.* **2008**, *188*, 153–165. [[CrossRef](#)]
47. Guan, Z.; Mu, S.; Li, H.; Jiang, T.; Zhang, M.; Wu, C. Flexible DEM model development and parameter calibration for rape stem. *Appl. Sci.* **2022**, *12*, 8394. [[CrossRef](#)]
48. Shen, C.; Li, X.; Tian, K.; Zhang, B.; Huang, J.; Chen, Q. Experimental analysis on mechanical model of ramie stalk. *Trans. Chin. Soc. Agric. Eng.* **2015**, *31*, 26–33.

Disclaimer/Publisher's Note: The statements, opinions and data contained in all publications are solely those of the individual author(s) and contributor(s) and not of MDPI and/or the editor(s). MDPI and/or the editor(s) disclaim responsibility for any injury to people or property resulting from any ideas, methods, instructions or products referred to in the content.